TURUN
YLIOPISTO
UNIVERSITY
OF TURKU

Porphyrin Based Electroactive Copolymers

From Electropolymerization to Energy and Environmental Applications

Sachin Kochrekar

TURUN YLIOPISTON JULKAISUJA – ANNALES UNIVERSITATIS TURKUENSIS
SARJA – SER. AI OSA – TOM. 764 | ASTRONOMICA – CHEMICA – PHYSICA – MATHEMATICA | TURKU 2026

TURUN
YLIOPISTO
UNIVERSITY
OF TURKU

PORPHYRIN BASED ELECTROACTIVE COPOLYMERS

From Electropolymerization to Energy and Environmental Applications

Sachin Kochrekar

TURUN YLIOPISTON JULKAISUJA – ANNALES UNIVERSITATIS TURKUENSIS
SARJA – SER. AI OSA – TOM. 764 | ASTRONOMICA – CHEMICA – PHYSICA – MATHEMATICA | TURKU 2026

University of Turku

Faculty of Science
Department of Chemistry
Chemistry
Doctoral programme in Exact Sciences (EXACTUS)

Supervised by

Professor Carita Kvarnström
Department of Chemistry
University of Turku
Turku Finland

Adjunct Professor Pia Damlin
Department of Chemistry
University of Turku
Turku Finland

Adjunct Professor Mikko Salomäki
Department of Chemistry
University of Turku
Turku Finland

Reviewed by

Dr. Aline Rougier
CNRS, University of Bordeaux
Bordeaux, France

Professor Laurent Ruhlmann
University of Strasbourg
Strasbourg, France

Opponent

Professor Eunkyoung Kim
Department of Chemical and
Biomolecular Engineering
Yonsei University
Seoul, South-Korea

The originality of this publication has been checked in accordance with the University of Turku quality assurance system using the Turnitin OriginalityCheck service.

ISBN 978-952-02-0735-9 (PRINT)
ISBN 978-952-02-0736-6 (PDF)
ISSN 0082-7002 (Print)
ISSN 2343-3175 (Online)
Painosalama, Turku, Finland 2026

Dedicated to my mother

To the woman who gave me strength before I knew weakness,
Hope before I knew fear,
And love before I understood sacrifice.

Every late night, every setback, every small victory
Carried the echoes of your prayers.

This thesis may bear my name,
But its foundation was built by your endless faith in me.

Mom, this achievement is not mine alone,
It is the story of your sacrifices written through
My journey.

UNIVERSITY OF TURKU
Faculty of Science
Department of Chemistry
Chemistry
SACHIN KOCHREKAR: Porphyrin Based Electroactive Copolymers,
From Electropolymerization to Energy and Environmental Applications
Doctoral Dissertation, 142 pp.
Doctoral Programme in Exact Sciences (EXACTUS)
June 2026

ABSTRACT

A material that exhibits both electrochromic properties and energy storage capabilities can directly address the UN's 2030 Agenda for Sustainable Development, given the global demand for cost-effective, environmentally friendly, and energy-efficient solutions.

This thesis describes an efficient electrocopolymerization approach for developing porphyrin-based copolymer thin film electrochromic supercapacitors. Three meso-aminophenyl porphyrins (MTAPP; M = Zn^{2+}, Ni^{2+}, H_2) are separately combined with 3,4-ethylenedioxythiophene (EDOT) via oxidative electrocopolymerization, yielding three copolymers: poly(NiTAPP-EDOT), poly(ZnTAPP-EDOT), and poly(H_2TAPP-EDOT). The MTAPP-EDOT copolymer thin films exhibit rapid electrochromic switching (< 2 s), significant optical contrast across the visible and beginning of the near-infrared regions, high coloration efficiency, and excellent open-circuit optical memory. The identity of the central metal ion strongly influences the electrochromic behavior and enables tuning of multicolor electrochromic responses. Poly(NiTAPP-EDOT) displays three distinct reversible color states, whereas poly(ZnTAPP-EDOT) and poly(H_2TAPP-EDOT) exhibit two distinct reversible color states. The three copolymer thin films were tested for electrochromic supercapacitor applications in 4 m $ZnCl_2$ aqueous electrolyte. To our knowledge, this is the first study of MTAPP-EDOT copolymer thin films in an aqueous electrolyte. Poly(NiTAPP-EDOT) exhibits electric-double-layer-capacitive-dominated characteristics, delivering a specific capacitance of 8.7 mF cm^{-2} and over 90% capacitance retention after 5000 galvanostatic charge-discharge cycles, while maintaining 100% Coulombic efficiency. Notably, poly(ZnTAPP-EDOT) and poly(H_2TAPP-EDOT) exhibit EDLC behavior, retaining 85% and 98% capacitance after 10,000 and 2,000 galvanostatic charge-discharge cycles, respectively.

Additionally, keto-functionalized octaethylporphyrins (MOEPK; M = Zn^{2+}, Ni^{2+}) are electropolymerized using 4,4′-bipyridine as a bifunctional bridging nucleophile, enabling direct polymerization without pre-functionalized monomers.

These findings provide new insights into structure-property relationships in porphyrin electropolymers and support their use in sustainable multifunctional electrochemical devices operating in water-based electrolyte systems.

KEYWORDS: Electrocopolymerization, Conducting polymers, Porphyrin, Electrochromism, Electrochromic supercapacitors

TURUN YLIOPISTO
Matemaattis-luonnontieteellinenTiedekunta
KemianLaitos
Kemia
SACHIN KOCHREKAR: Porfyriinipohjaiset elektroaktiiviset kopolymeerit: sähkökemiallisesta polymeroinnista energia- ja ympäristösovelluksiin.
Väitöskirja, 142 s.
Eksaktien tieteiden tohtoriohjelma (EXACTUS)
Kesäkuu 2026

TIIVISTELMÄ

Materiaali, jolla on sekä sähkökromisia ominaisuuksia että energianvarastointikykyä, voi suoraan edistää YK:n kestävän kehityksen Agenda 2030 -tavoitteita vastaten maailmanlaajuiseen tarpeeseen kehittää kustannustehokkaita, ympäristöystävällisiä ja energiatehokkaita ratkaisuja.

Tässä väitöskirjassa esitetään tehokas sähkökemiallinen kopolymerisaatiomenetelmä porfyriinipohjaisten kopolymeerikalvojen valmistamiseksi sähkökromisia superkondensaattoreita varten. Kolme meso-aminofenyyli-porfyriiniä (MTAPP; M = Zn^{2+}, Ni^{2+}, H_2) yhdistetään 3,4-etyleenidioksitiofeeniin (EDOT) hapettavan sähkökemiallisen kopolymeroinnin avulla muodostaen kolme kopolymeeria: poly(NiTAPP-EDOT), poly(ZnTAPP-EDOT) ja poly(H_2TAPP-EDOT). MTAPP-EDOT-kopolymeerikalvoilla on nopea sähkökrominen värinvaihto (< 2 s), merkittävä optinen kontrasti, korkea värjäytymistehokkuus sekä erinomainen optinen muisti. Keskusmetalli-ioni vaikuttaa voimakkaasti sähkökromiseen käyttäytymiseen ja mahdollistaa monivärisen vasteen: poly(NiTAPP-EDOT) kykenee kolmeen palautuvaan väritilaan, kun taas poly(ZnTAPP-EDOT) ja poly(H_2TAPP-EDOT) kahteen. Kolmea kopolymeerikalvoa testattiin sähkökromisina superkondensaattoreina vesipohjaisessa elektrolyyttiliouksessa (4 m $ZnCl_2$), mikä on tietojemme mukaan ensimmäinen tutkimus MTAPP-EDOT-kopolymeereistä vesipohjaisessa elektrolyytissä. Poly(NiTAPP-EDOT) osoittaa kaksoiskerroskapasitanssikäyttäytymistä, saavuttaen ominaiskapasitanssin 8,7 mF cm^{-2} ja yli 90 % kapasitanssin säilymisen 5000 syklin jälkeen 100 % Coulombisella hyötysuhteella. Poly(ZnTAPP-EDOT) ja poly(H_2TAPP-EDOT) säilyttävät vastaavasti 85 % ja 98 % kapasitanssista.

Lisäksi keto-funktionalisoituja oktaetyyliporfyriinejä (MOEPK; M = Zn^{2+}, Ni^{2+}) sähköpolymeroitiin käyttäen 4,4′-bipyridiiniä nukleofiilisenä siltana ilman esifunktionalisoituja monomeerejä.

Tulokset syventävät ymmärrystä porfyriinipohjaisten polymeerien rakenne-ominaisuussuhteista ja tukevat niiden käyttöä kestävissä, monitoimisissa sähkökemiallisissa laitteissa vesipohjaisissa elektrolyyteissä.

ASIASANAT: Sähköpolymerisaatio, Johtavat polymeerit, Porfyriini, Sähkökromismi, Sähkökromiset superkondensaattorit

Table of Contents

Abbreviations

AFM	Atomic force microscopy
ACN	Acetonitrile
Ag/AgCl	Silver/Silver chloride
bNIR	Beginning of the near-infrared
CBZ	Carbazole
CE	Coloration efficiency
CE	Counter electrode
CIE	Commission Internationale de l'Éclairage
CPs	Conducting polymers
CV	Cyclic voltammetry
CT	Charge transfer
DFT	Density functional theory
DCE	1,2-dichloroethane
EC	Electrochromic
ECD	Electrochromic device
ECSCs	Electrochromic supercapacitors
EDLC	Electric double-layer capacitance
EDOT	3,4-ethylenedioxythiophene
ESR	Equivalent series resistance
FTIR	Fourier transform infrared
FTO	Fluorinated tin oxide
GC	Glassy carbon
GCD	Galvanostatic charge-discharge
HOMO	Highest occupied molecular orbital
KCl	Potassium chloride
LUMO	Lowest unoccupied molecular orbital
TOEPK	Tetraoctaethylporphyrin ketone
NIR	Near-infrared
OD	Optical density
PANI	Poly(aniline)
PAz	Poly(azulene)

PEDOT	Poly(3,4-ethylenedioxythiophene)
PTh	Polythiophene
Pz	Phenazine
PzH_2	Dihydrophenazine
RE	Reference electrode
SEM	Scanning electron microscopy
$TBAPF_6$	Tetrabutylammonium hexafluorophosphate
TD-DFT	Time-dependent density functional theory
TAPP	Tetraaminophenyl porphyrin
TPA	Triphenylamine
UV-Vis	Ultraviolet-visible
WE	Working electrode
XPS	X-ray photoelectron spectroscopy
$ZnCl_2$	Zinc chloride
4,4′-bpy	4,4′-bipyridine

Symbols

A	Area
a*	Red-green
Ag	Silver
Ar	Argon
b*	Yellow-blue
C	Capacitance
CO_2	Carbon dioixde
F	Farad
L*	Lightness
m	Molality
M	Molarity
mF	Millifarad
N_2	Nitrogen
I	Current
R	Resistance
T	Transmittance
V	Potential
α	alpha
β	beta
π	pi
η	eta
λ	lambda
μ	mu
σ	sigma
υ	upsilon
ν	Scan rate
Δ	delta

List of Original Publications

This dissertation is based on the following original publications, which are referred to in the text by their Roman numerals:

I **Sachin, Kochrekar**, Plawan Kumar Jha, Subrahmanyam Sappati, Ermei Mäkilä, Ashwini Jadhav, Pia Damlin, Mikko Salomäki, and Carita Kvarnström. Electrocopolymerized NiTAPP-EDOT Thin Film with Fast Electrochromic Response and High Supercapacitive Performance in Aqueous Electrolyte (Submitted).

II **Sachin, Kochrekar,** Subrahmanyam Sappati, Plawan Kumar Jha, Ermei Mäkilä, Ashwini Jadhav, Pia Damlin, Mikko Salomäki, and Carita Kvarnström. Ultrafast Ampipolar Switching in Electrochromic Copolymer Thin Films of Zinc (II) Tetrakis (4-aminophenyl) porphyrin-3, 4-ethylenedioxythiophene. *Journal of Materials Chemistry C,* 2025, 13(47): 23577-23588. https://doi.org/10.1039/D5TC03045E

III **Sachin, Kochrekar**, Ajit, Kalekar, Shweta Mehta, Pia Damlin, Mikko Salomäki, Sari Granroth, Niko Meltola, Kavita Joshi, and Carita Kvarnström. Copolymers of bipyridinium and metal (Zn & Ni) porphyrin derivatives; theoretical insights and electrochemical activity towards CO_2. *RSC advances,* 2021, 11(32): 19844-19855. https://doi.org/10.1039/D1RA01945G

List of Other Publications

I Plawan Kumar Jha, **Sachin Kochrekar**, Ashwini Jadhav, Robert Lassfolk, Mikko Salomäki, Ermei Mäkilä, and Carita Kvarnström. Wide electrochemical stability window of $NaClO_4$ water-in-salt electrolyte elevates the supercapacitive performance of poly (3,4-ethylenedioxythiophene). *Energy Storage Materials,* 2024, 72: 103758. https://doi.org/10.1016/j.ensm.2024.103758

II Narhari Sapkota, Plawan Kumar Jha, Anssi Peuronen, **Sachin Kochrekar**, Ermei Mäkilä, Carita Kvarnström, and Ari Lehtonen. Supercapacitive Performance of a PEDOT⊃Metal-Porphyrin Framework Composite in a Concentrated Aqueous $LiClO_4$ Electrolyte. *Journal of Materials Chemistry C,* 2026, 14(2): 796-805. https://doi.org/10.1039/D5TC03251B

III Ashwini Jadhav, Plawan Kumar, Jha, Pia Damlin, **Sachin Kochrekar**, Mikko Salomäki, and Carita Kvarnström. Redox-Coupled $ZnCl_2$ Water-in-Salt Electrolyte Enables High-Capacity and Ultrastability in 2D Ti_3C_2Tx MXene Supercapacitor (submitted).

IV **Sachin Kochrekar**, Plawan Kumar Jha, Pia Damlin, Mikko Salomäki, and Carita Kvarnström. Electrochromic Supercapacitor Performance and in Situ UV-Vis and Raman Spectroscopic Studies of poly(ZnTAPP-EDOT) in Concentrated Aqueous Electrolyte (to be submitted).

V **Sachin Kochrekar**, Plawan Kumar Jha, Pia Damlin, Mikko Salomäki, and Carita Kvarnström. Electrocopolymerized Poly(H_2TAPP-EDOT) Thin Films as Electrochromic Supercapacitors in Concentrated Aqueous Electrolyte (to be submitted).

VI Plawan Kumar Jha, **Sachin Kochrekar,** Ashwini Jadhav**,** Reman Kumar Singh, Pia Damlin, Siyuan Peng, Santosh Kumar Singh, Mikko Salomäki, and Carita Kvarnström. Improving Supercapacitive Performance of PEDOT-rGO Nanocomposite by Concentrated Aqueous Electrolyte (to be submitted).

1 Introduction

Smart materials and intelligent solutions are among the key drivers of next-generation energy and electronic systems. The remarkable manifestations of nature have long been a significant source of inspiration and guidance for scientific innovation, from fundamental insights to technological applications. Biological systems have inspired numerous ideas for synthetic materials. For example, adhesive materials based on the structure of gecko feet, self-cleaning and superhydrophobic surfaces inspired by lotus leaves, and materials that replicate the high strength and elasticity of spider silk[1–4]. In addition, the remarkable ability of organisms such as octopuses and chameleons to change color in response to their environment has driven interest in chromic materials[5]. These examples demonstrate how nature-inspired, adaptive, and responsive materials, now known as smart materials, provide new design strategies for advanced technologies[1].

Smart materials, also referred to as intelligent or advanced materials, are a class of functional materials that can reversibly alter physical, chemical, or optical properties in response to external stimuli in a controlled manner, thereby making them highly versatile and adaptable[6,7]. Owing to their responsive and adaptive behavior, smart materials have found widespread applications across diverse fields, including medicine, healthcare, robotics, aerospace, automotive engineering, construction, and consumer electronics, where they enable enhanced performance, functionality, and adaptability[8]. From a functional perspective, smart materials can be broadly classified into passive and active systems based on their interaction with energy[9]. Passive smart materials primarily facilitate the transmission or guidance of energy without undergoing intrinsic property changes. In contrast, active smart materials respond directly to external stimuli and either exhibit reversible changes in their properties or convert one form of energy into another. An overview of the principal categories of smart materials and their characteristic stimulus-response behaviors is provided in Table 1[7–10].

The growing interest in multifunctional smart materials has driven the development of systems capable of integrating complementary properties within a single platform, offering advantages in terms of performance, cost-effectiveness, and device compactness. Accordingly, the electrochromic material investigated in this

work was also evaluated for its energy-storage performance using supercapacitor studies. Global energy demandcontinues to rise due to population growth, economic development, and the increasing adoption of energy-intensive technologies. Despite improvements in energy efficiency, higher living standards and industrial activity still drive overall energy consumption. Environmental concerns and the limited availability of fossil fuels have accelerated the transition toward renewable and low-carbon energy sources. While recent advances in renewable technologies provide significant sustainability benefits, their large-scale integration into existing energy systems remains challenging. This is mainly due to intermittent energy generation, dependence on environmental conditions, and uneven geographical distribution. These challenges underscore the need for advanced materials and system design strategies that can enhance the stability, efficiency, and reliability of future energy systems.

Table 1. Classification of smart materials based on external stimuli-response behavior[7–10].

Types of smart materials	Primary external stimuli/ Stimulus	Characteristic response/ behavior	Typical applications
Piezoelectric materials	Mechanical stress, electrical field	Generates an electric charge under mechanical stress or deforms under an applied electric field	Sensors, actuators, energy harvesting devices
Shape memory alloys (SMAs)	Temperature, mechanical stress	Recovers a predefined shape upon thermal or mechanical activation	Actuators, biomedical stents, aerospace components
Electrostrictive materials	Electric field	Exhibits reversible strain proportional to the square of the applied electric field	Precision actuators, adaptive optics
Magnetostrictive materials	Magnetic field	Undergoes dimensional changes in response to a magnetic field	Actuators, vibration control systems
Chromic materials	Electrical, optical, thermal, or mechanical	Reversible changes in color or optical properties	Smart windows, displays, sensors
Magnetorheological fluids	Magnetic field	Rapid and reversible changes in viscosity	Dampers, clutches, vibration control
Electrorheological fluids	Electric field	Reversible changes in viscosity under an applied electric field	Adaptive dampers, robotics

1.1 Chromic Materials

Among different smart materials, optically responsive or chromic materials have attracted significant attention due to their ability to reversibly modulate color or optical properties in response to external stimuli. The observed color originates from changes in their electronic structure. Based on the nature of the stimulus, chromic materials can be broadly classified into photochromic, thermochromic, mechanochromic, and electrochromic systems, which respond to light, temperature, mechanical stress, and electrical potential, respectively (Figure 1) [7,11]. In addition, other chromic systems include gasochromic (responsive to gaseous species), biochromic (triggered by biological stimuli), chemochromic (induced by chemical interactions), and solvatochromic materials (responsive to the solvent polarity changes) [7,11].

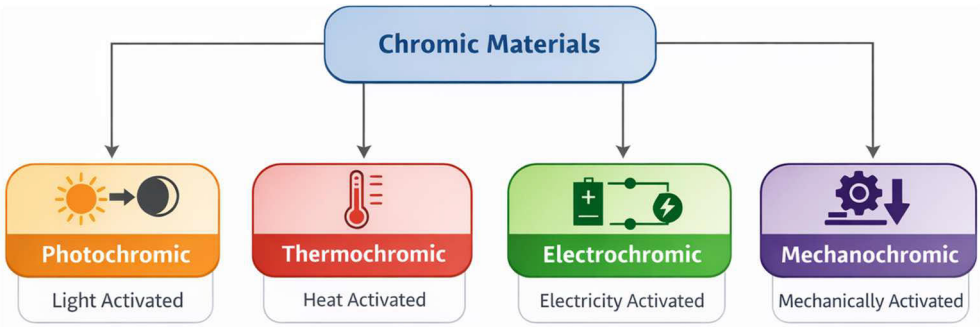

Figure 1. Classification of chromic materials based on the nature of the external stimulus[8,11].

1.2 Electrochromism and Electrochromic (EC) Materials

Electrochromism refers to a phenomenon in which a material undergoes a reversible and persistent change in color or optical transmittance upon application of an electrical stimulus. This behavior originates from electrochemically induced redox processes that modify the electronic structure of the material and, consequently, its interaction with light[12–14]. Materials that exhibit this effect are known as EC materials.

The term “electrochromism” was formally introduced by John R. Platt in 1961, marking the beginning of systematic scientific investigation into electrically driven optical modulation[15]. Shortly thereafter, Satyen K. Deb reported the first practical demonstrations of EC materials and devices while investigating amorphous and crystalline transition metal oxides at the American Cyanamid Company[16,17]. These studies established tungsten oxide-based systems as prototypical EC materials and

laid the foundation for modern electrochromic device development. Systematic investigations of electrochromism expanded during the mid-twentieth century, as advances in electrochemistry and solid-state science enabled controlled studies of electrically induced optical changes. Research gradually evolved from simple observations of color change towards understanding the redox processes and charge-transport mechanisms underlying EC behavior[18–20]. This growing mechanistic insight, together with improvements in material processing and device design, enabled EC systems to progress beyond laboratory demonstrations and toward practical implementations.

EC materials are particularly advantageous due to their precise controllability, low power consumption, and compatibility with electrochemical systems. Unlike photochromic or thermochromic materials, whose responses are governed by environmental conditions, EC materials allow direct and reversible modulation of optical properties through an applied electrical stimulus[4]. This unique combination of electrical control and optical functionality makes EC materials especially attractive for applications in smart windows, displays, and energy storage devices[18,19,21,22]. The progression of electrochromic materials over the years, highlighting major developments, is illustrated in Figure 2.

1.3 Classification of EC Materials

Electrochromic materials can be classified based on their operational characteristics, structural behavior, and practical applications. This classification is illustrated schematically in Figure 3.

1.3.1 Redox State Solubility

One widely adopted classification scheme categorizes electrochromes into Type I, Type II, and Type III systems based on the solubility of their redox states during operation[23,24]. Type I electrochromic materials contain both oxidized and reduced species that remain soluble, and the electrochromic response occurs in solution through diffusion-controlled electron transfer at the electrode interface. As a result, continuous charge injection is required to maintain the colored state. Type II electrochromic materials are soluble in their initial state but become insoluble upon redox conversion, resulting in the formation of a colored deposit on the electrode surface and exhibiting optical memory. In contrast, Type III electrochromic materials remain in the solid state throughout the electrochromic process, with color changes occurring within solid films deposited on electrode surfaces. Due to their solid-state operation and optical memory, Type III materials are particularly relevant for practical EC applications[23,24].

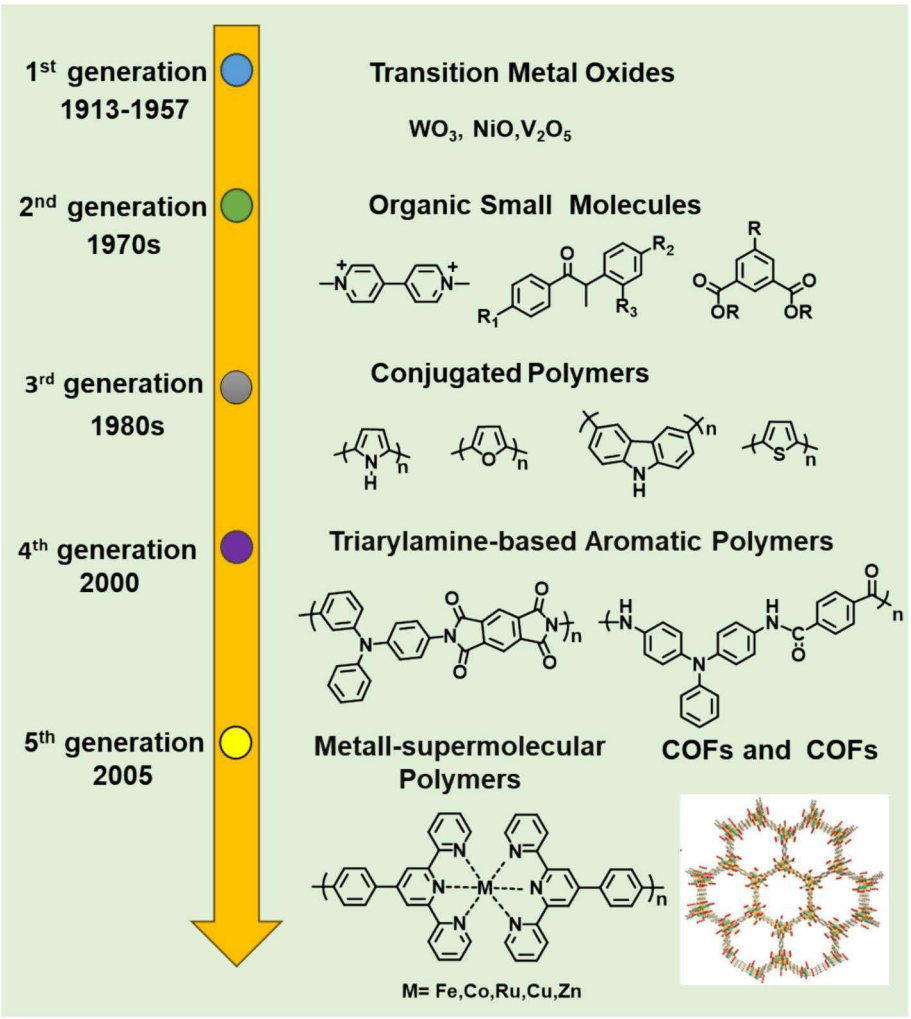

Figure 2. Timeline on the development of electrochromic materials[25].

1.3.2 Color-Change Properties

EC materials can also be categorized according to their optical response during electrochemical redox switching. Based on color-transition characteristics, EC systems are commonly divided into three categories: (a) bleaching-coloration systems: reversibly switch between a colored and a transparent state, (b) dual-color systems: switch between two distinct colored states, and (c) multicolor or polyelectrochromic systems: multiple electrochemically accessible redox states give rise to several optically distinguishable color states. This polyelectrochromic behavior is particularly pronounced in conjugated polymer-based electrochromic systems[26].

1.3.3 Electrochemical Response

EC materials can be classified according to their color-changing mechanism under applied bias. Materials that undergo coloration upon oxidation are termed anodic (p-type), whereas those that exhibit coloration upon reduction are referred to as cathodic (n-type) EC materials[26,27].

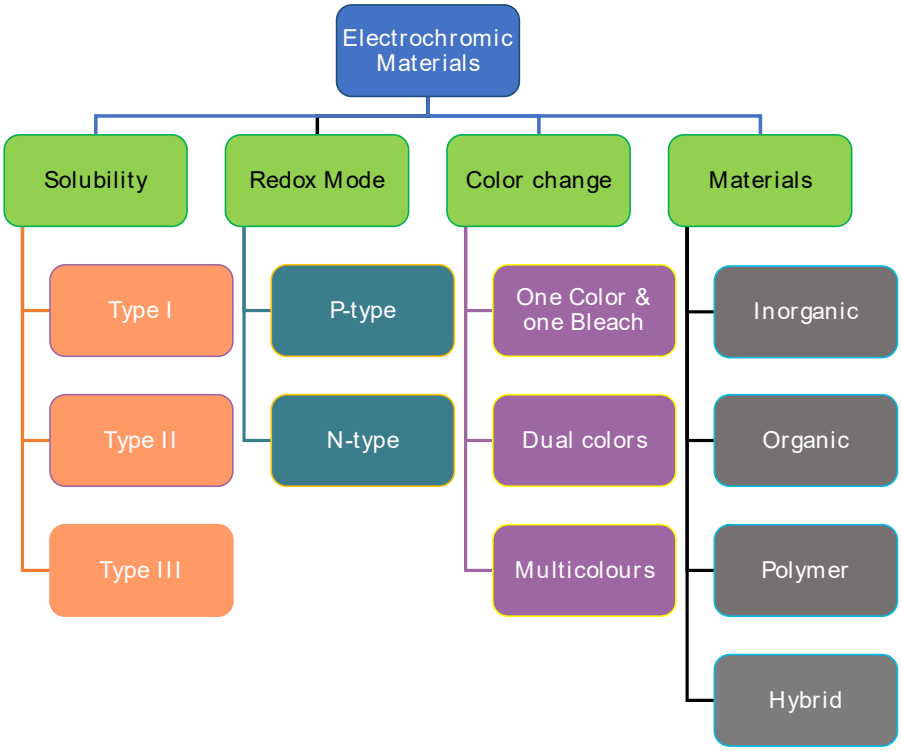

Figure 3. Classification of electrochromic materials.

1.3.4 Materials Composition and Chemical Nature

EC materials are also classified according to their material composition and chemical nature, which strongly influence their redox behavior, optical properties, processability, and stability. Based on composition, EC materials can be broadly categorized as:

(a) Inorganic EC materials include transition metal compounds, such as tungsten oxide (WO_3), nickel oxide (NiO), and molybdenum oxide (MoO_3), as well as metal hexacyanometallates such as Prussian blue. These materials exhibit electrochromism through changes in metal oxidation states coupled with ion insertion or extraction. They also show chemical robustness and long-term cycling stability[28,29].

(b) Organic EC materials consist of small organic molecules or metal-organic complexes that undergo reversible redox reactions accompanied by changes in electronic structure or conjugation length. These materials offer structural diversity and tunable optical properties; however, their practical use may be limited by solubility and stability[28,29].
(c) Polymeric EC materials, including conjugated polymers and metallopolymers, represent a highly versatile class of EC materials. Their extended conjugated backbones and distributed redox-active sites enable efficient charge delocalization, pronounced optical modulation, and access to multiple redox states. Furthermore, polymeric systems offer mechanical flexibility and processability, making them particularly attractive for advanced electrochromic applications[29,30].
(d) Hybrid EC materials combine two or more types of materials. For example, they include inorganic-organic, polymer-inorganic, and metal-organic systems. By coupling the structural stability of inorganic materials with the tunability and flexibility of organic or polymeric constituents, hybrid EC materials can exhibit enhanced optical contrast, improved charge transport, and multifunctional behavior. Such hybrid architectures are increasingly explored for next-generation EC and energy-related applications[28,29].

1.4 Electrochromic Characteristics

Electrochromic characteristics in materials originate from electrochemically driven redox reactions that induce reversible changes in their electronic structure, resulting in the modulation of their optical properties[31]. To maintain overall charge neutrality, this electronic charge transfer is accompanied by the ingress or egress of charge-compensating ions from the surrounding medium. These coupled electron and ion transfer processes alter the population and distribution of electronic states within the material. As a result, the optical absorption characteristics of the material change across UV-Vis-NIR regions, giving rise to visible changes in optical transmittance[32]. The reversible transition between these states is referred to as the coloration-bleaching process. Coloration corresponds to the formation of a redox state associated with enhanced optical absorption within a specific spectral region, whereas bleaching involves the reverse redox process, restoring a lower-absorption state or an alternative optical appearance[33]. The reversibility of these redox-induced optical changes is a defining characteristic of EC materials, along with long-term cycling stability without irreversible chemical transformation[30]. The kinetics of electrochromic response are governed by intrinsic properties such as electrical conductivity, ion mobility, and the density of redox-active sites.

In addition to optical modulation, some EC materials inherently exhibit electrochemical charge storage behavior. This intrinsic coupling between optical

response and charge storage at the material level provides a fundamental basis for the development of multifunctional systems[34].

1.5 Multifunctional Electrochromic Materials

Multifunctional EC materials can perform multiple functions within a single material framework, and have emerged as an important research area, driven by the growing demand for advanced and sustainable materials[35]. A primary motivation for developing multifunctional EC materials is the enhancement of efficiency, utility, and sustainability[21,27,35,36]. When EC materials are integrated with other active functionalities, they give rise to multifunctional smart materials, suitable for energy and environmental applications. For example, they can be engineered to incorporate additional functional attributes such as energy storage capability, sensing functionality, optical emission, and mechanical flexibility[37].

Among these, materials that simultaneously exhibit optical modulation and charge storage are of particular interest. In such systems, the same redox-active sites responsible for color change also participate in reversible charge accumulation, enabling real-time visual monitoring of the electrochemical state. This intrinsic coupling between electrochromism and charge storage underpins the development of electrochromic supercapacitor materials[34,37,38].

1.6 Supercapacitors (SCs)

Supercapacitors (SCs), also known as electrochemical capacitors or ultracapacitors, represent an important class of energy storage devices that bridge the gap between conventional capacitors and batteries[39,40]. They offer high power density, rapid charge-discharge rates, excellent cycling stability, and long operational lifetimes. Unlike batteries, supercapacitors store charge primarily at or near the electrode-electrolyte interface, enabling faster kinetics and superior reversibility. These features make them particularly attractive for applications requiring quick bursts of power, such as regenerative braking systems, peak power assistance, backup power supplies, and portable electronics. However, supercapacitors typically exhibit lower energy density compared to batteries, which has driven extensive research into advanced electrode materials and hybrid systems. The overall performance of supercapacitors depends on their charge storage mechanism, electrode material properties, electrolyte composition, and device architecture. Current research efforts focus on enhancing energy density while preserving their inherent advantages in power delivery and long cycle life[41,42].

1.6.1 Charge Storage Mechanisms in Supercapacitors

Supercapacitors store electrical energy through two primary mechanisms: electric double-layer capacitance (EDLC) and pseudocapacitance. EDLC is a non-faradaic process where charge accumulates electrostatically at the electrode-electrolyte interface. When a potential is applied, ions from the electrolyte migrate and adsorb onto the electrode surface, forming two layers of opposite charges separated by a molecular-scale distance (the Helmholtz layer)[41]. This purely electrostatic charge separation is highly reversible and enables exceptionally fast charge-discharge kinetics. Carbon-based materials such as activated carbon, carbon nanotubes, and graphene are commonly employed for EDLC due to their high surface area and excellent conductivity[43]. Pseudocapacitance, in contrast, involves fast and reversible faradaic redox reactions occurring at or near the electrode surface. Unlike battery-type processes that involve bulk phase transformations, pseudocapacitive charge storage occurs through surface or near-surface redox processes, intercalation, or electrosorption[41]. These processes produce capacitive-like behavior with quasi-linear charge-voltage characteristics. Transition metal oxides (RuO_2, MnO_2), conducting polymers (polyaniline, polypyrrole, PEDOT), and heteroatom-doped carbons exhibit pseudocapacitive behavior and generally provide higher specific capacitance than purely EDLC materials, though often with reduced cycling stability[42,44].

1.7 Electrochromic Supercapacitors (ECSCs)

Electrochromic materials and supercapacitors are both governed by electrochemical redox reactions involving reversible ion and electron transport within electrode materials. In electrochromic systems, these redox processes manifest as changes in optical properties, whereas in supercapacitors, they enable reversible energy storage. The shared electrochemical nature of these processes provides a fundamental basis for combining electrochromic and energy storage functionalities at the materials level[34,45].

ECSCs represent a multifunctional material concept in which electrochromic behavior and electrochemical energy storage are realized within the same electrode material. In such materials, reversible redox reactions lead to both charge accumulation and optical modulation, enabling visual indication of the electrochemical state through color changes[46]. This intrinsic coupling between optical response and charge storage distinguishes electrochromic supercapacitor (ECSC) materials from conventional supercapacitor electrodes and electrochromic materials designed solely for optical modulation[47,48]. Many electrochromic materials, particularly those exhibiting pseudocapacitive behavior, inherently possess charge storage capability. As a result, various redox-active materials, including transition

metal oxides, conducting polymers, and hybrid organic-inorganic systems, have been explored as electrode materials for ECSCs[48,49]. Despite growing research interest, several challenges remain, including limited energy density, insufficient cycling stability, and incomplete coupling between optical and electrochemical performance. Addressing these limitations requires careful consideration of electrode material composition, structural design, electrolyte selection, and redox activity, highlighting the importance of materials selection and design in advancing electrochromic supercapacitor performance.

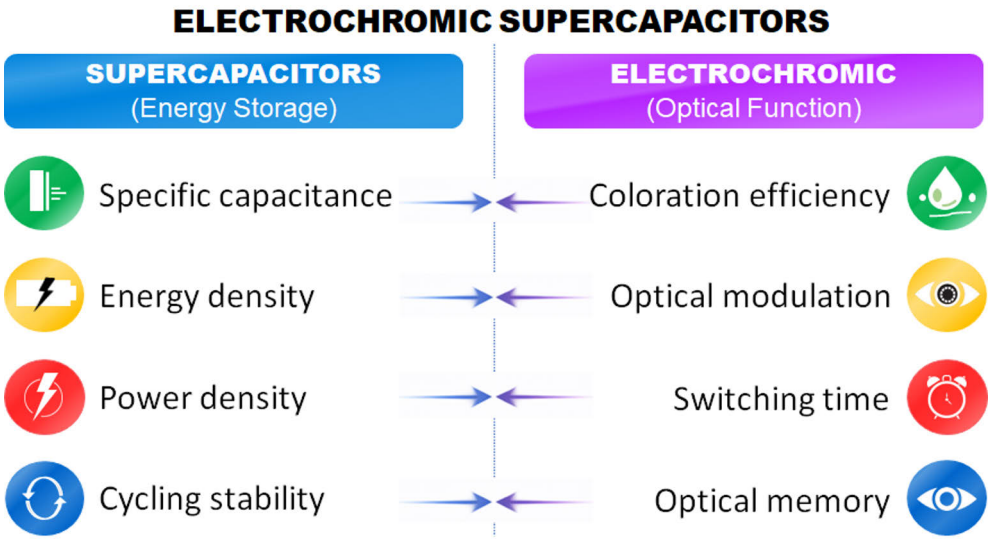

Figure 4. Performance parameter for Electrochromic supercapacitors (ECSCs).

1.8 Performance Parameters of Electrochromic Supercapacitor Materials

The performance of ECSC materials is evaluated using a combination of optical and electrochemical parameters that describe the efficiency, reversibility, stability, and visual effectiveness of their color modulation and charge storage behavior. These parameters provide a quantitative framework for comparing different material systems and for assessing their suitability for practical and multifunctional applications[50].

1.8.1 Optical Contrast

Optical contrast (Δ%T) is typically expressed as the difference in transmittance (%) between the fully oxidized and fully reduced states and is defined as:

$$\Delta\%\mathrm{T} = T_{ox} - T_{red} \quad \text{(a)}$$

where T_{ox} and T_{red} represent the transmittance values in the oxidized and reduced states, respectively.

1.8.2 Switching (Response) Time

It is defined as the time required for the material to reach 90% of its total transmittance change during coloration or bleaching. Fast switching is particularly important for applications requiring dynamic optical modulation, such as smart windows, adaptive displays, and switchable mirrors.

1.8.3 Coloration Efficiency

Coloration efficiency (*CE*) quantifies the optical density change produced per unit of electronic charge injected or extracted from the electroactive film. The optical density change (ΔOD) between the oxidized and reduced states is given by:

$$\Delta OD = \log {}^{T_{ox}}/_{T} \quad \text{(b)}$$

The coloration efficiency (η) can be expressed as:

$$CE = {}^{\Delta \mathrm{OD}}/_{Q_{\mathrm{d}}} \quad \text{(c)}$$

where Q_d represents the charge density (C cm^{-2}), CE, typically reported in cm^2 C^{-1}, reflects how effectively the injected charge is utilized to produce an optical change.

1.8.4 Optical Memory (open-circuit memory)

Optical memory, also referred to as open-circuit memory, describes the ability of an electrochromic material to retain its optical state after the external potential is removed. It is evaluated by monitoring the temporal evolution of transmittance or absorbance under open-circuit conditions following electrochemical switching. Strong optical memory indicates minimal spontaneous relaxation or ion back-diffusion once the applied potential is removed.

1.8.5 CIE colorimetry

CIE colorimetry provides a quantitative framework for describing and comparing color changes in electrochromic materials during redox switching. It is based on the CIELAB (L*a*b*) color space, where L* represents lightness, and a* and b*

correspond to the red-green and yellow-blue chromatic axes, respectively. The total color difference (ΔE*) between two optical states is calculated as:

$$\Delta E^* = ((\Delta L^*)^2 + (\Delta a^*)^2 + (\Delta b^*)^2)^{1/2} \quad \text{(d)}$$

1.8.6 Mathematical equations for supercapacitors

Electrochemical performance of a supercapacitor can be evaluated using cyclic voltammetry (CV), Galvanostatic charge-discharge (GCD), and electrochemical impedance spectroscopy (EIS) techniques[51].

$$From\ GCD;\ C = \frac{Charge\ (Q)}{Potential\ (V)} = \frac{I*t}{V} = \frac{I}{slope} \quad \text{(e)}$$

$$From\ CV;\ C = \frac{\int_{v1}^{v2} \mathrm{I(V)\ dV}}{\mathrm{V}*\frac{\mathrm{dv}}{\mathrm{dt}}} \quad \text{(f)}$$

Where,
C → capacitance of the electrode active material (in farad (F)); I → current (in amperes (A));
t → discharge time excluding voltage IR drop (in s); $\int_{v1}^{v2} \mathrm{I(V)\ dV}$ → Average current from anodic or cathodic sweep extracted from CV;
$\frac{\mathrm{dv}}{\mathrm{dt}}$ → scan rate (in V s^{-1}); V → the potential window in volts.

$$\text{Energy density } (\mathrm{E}_d) = \frac{1}{2} * C * V^2\ (in\ Wh\ kg^{-1}) \quad \text{(g)}$$

$$\text{Power density } (\mathrm{P}_d) = \frac{\mathrm{E}_d}{t_{discharge}}\ (in\ W\ kg^{-1}) \quad \text{(h)}$$

1.9 Conducting Polymers (CPs)

Conducting Polymers (CPs) are particularly attractive for ECSCs due to their conjugated structures, multiple accessible redox states, fast charge transport, easy thin film processing, and intrinsic electrochromic behavior[50,52]. These characteristics enable efficient charge storage along with pronounced and tunable optical modulation[46]. Furthermore, the structural versatility of CPs allows precise tuning of their electrochemical and optical properties through molecular design, rendering them highly adaptable functional materials[53,54].

The electrochromic behavior of CPs is governed by their delocalized π-conjugated backbone[54,55]. In the neutral state, CPs typically absorb strongly in the visible region, resulting in intense coloration. Upon electrochemical oxidation, charge carriers are introduced through doping, modifying the electronic structure and shifting the absorption band toward longer wavelengths. This spectral shift produces distinct color changes or bleaching, forming the basis of their electrochromic

response[40,56]. Importantly, the same electrochemical doping and de-doping processes responsible for optical modulation also enable reversible charge storage within the polymer matrix, often through pseudocapacitive mechanisms[50,57]. Consequently, CPs are well-suited as multifunctional electrochromic energy storage materials. Their structural tunability can be achieved through modifications at both molecular and macroscopic levels, including variation in the polymer backbone, side-chain engineering, and incorporation of different electroactive units[39,40,50].

The synthesis of CPs plays a crucial role in determining their electrochemical, optical, and structural properties. A wide range of synthetic strategies have been developed to prepare CPs with controlled molecular structure, morphology, and redox behavior. These include vapor-phase polymerization, oxidative chemical vapor deposition, hydrothermal methods, template-assisted approaches, electrospinning, self-assembly, interfacial polymerization, plasma polymerization, chemical polymerization, and electropolymerization[53,57]. Among these, chemical and electrochemical polymerizations remain the most widely employed methods. Chemical polymerization is particularly suitable for large-scale synthesis and backbone modification, whereas electrochemical polymerization offers superior control over film thickness, morphology, and electrochemical properties. Owing to its simplicity, reproducibility, low cost, and environmentally benign nature, electropolymerization has been extensively employed for the fabrication of conducting polymer films for electrochromic and supercapacitor studies[58].

CPs such as polyaniline (PANI), polyazulene (PAz), polyfuran, polyphenylene, polycarbazole, polypyrrole (PPy), polythiophene (PTh), and their derivatives, can be synthesized both chemically and electrochemically[40,50]. They are widely studied due to their favorable electrochemical activity, electrical conductivity, and chemical and mechanical stability[40,59,60].

Amongst polythiophene derivatives, poly(3,4-ethylenedioxythiophene) (PEDOT) has attracted particular attention owing to its high electrical conductivity, excellent environmental and electrochemical stability, optical transparency in the doped state, and good biocompatibility[61]. These attributes have established PEDOT as a widely used material in multifunctional electrochemical applications, including ECSCs[62]. PEDOT-based systems have demonstrated efficient electrochromic modulation and high capacitance over a wide voltage range, making them compatible with both aqueous and organic electrolytes and suitable for copolymer design strategies[63].

Since the first report of EDOT electrochemical polymerization in 1991[64], a large family of EDOT derivatives with tailored side-chain modifications has been synthesized and investigated[61,65]. This progress has naturally led to the development of EDOT-based copolymer systems that enable tuning of electronic structure, mechanical robustness, and color-switching behavior[66,67]. To introduce

complementary functionalities such as enhanced charge carrier mobility, increased pseudocapacitance, and expanded optical tunability, EDOT has been copolymerized with a broad range of conjugated and redox-active heterocycles[68,69], including carbazole[70,71], aniline[72], thiophene[73], diazoles[71], triazoles[71,74], indole[75], and triphenylamine[76] derivatives. Moreover, this molecular design strategy can be extended to macrocyclic and highly conjugated systems, such as porphyrins, which offer unique structural and electronic features that further expand the functional capabilities of EDOT-based electrochromic and energy storage materials.

1.9.1 Porphyrins as Electroactive Building Blocks

Porphyrins constitute a distinctive class of heterocyclic tetrapyrrolic macrocycles and are among the most widespread and functionally important molecules in nature. The term *porphyrin* originates from the ancient Greek word *porphura*, meaning purple, reflecting the intense coloration commonly exhibited by these macrocyclic systems[76]. Structurally, porphyrins consist of a fully conjugated macrocyclic ring formed by four pyrrole units interconnected through methine (=CH-) bridges, resulting in a highly aromatic 18 π-electron system. The central cavity, defined by the nitrogen atoms of the pyrrole rings, serves as a coordination site for metal ions, enabling the formation of metalloporphyrins with diverse electronic, catalytic, and redox properties[77]. Beyond their biological significance, porphyrins are highly versatile electroactive building blocks. Their extended π-conjugation, accessible redox states, and multiple reactive sites make them particularly attractive for electrochemical applications[78,79].

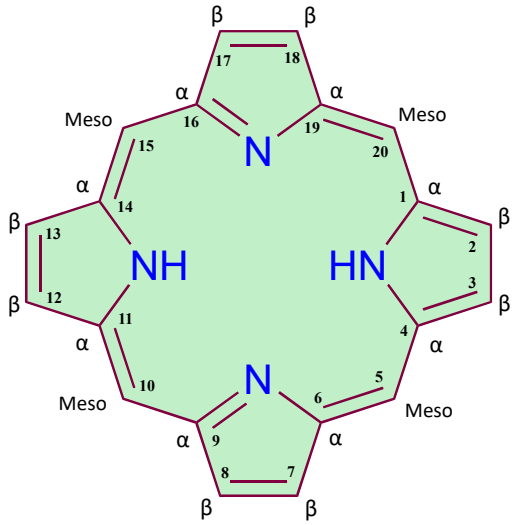

Figure 5. A Schematic representation of a porphyrin macrocycle.

1.9.2 Electropolymerization of Porphyrins

Several strategies, including chemical oxidative coupling, coordination polymerization, and electrochemical methods, have been developed for the polymerization of porphyrins[79,80]. Among these, electropolymerization has emerged as a particularly advantageous approach due to its ability to produce uniform, adherent polymer films directly on electrode surfaces with precise control over film thickness and morphology[80–82]. Owing to their extended π-conjugation and multiple reactive sites, porphyrins can undergo electropolymerization through electrochemical oxidation, which generates reactive radical cation species. These intermediates couple at the meso-positions (5, 10, 15, and 20), or at the β-pyrrolic positions (2, 3, 7, 8, 12, 13, 17, and 18), resulting in the formation of extended conjugated polymeric networks while largely preserving the aromatic integrity of the porphyrin core (Figure 5)[30]. Based on their structural features, the electropolymerization of porphyrins can be broadly classified according to the presence or absence of electroactive substituents at the macrocycle periphery (Figure 6). Porphyrins lacking electroactive substituents generally require external nucleophilic linkers or bridging units to facilitate polymer growth. In contrast, porphyrins functionalized with electroactive groups can undergo direct self-polymerization or electrocopolymerization with other conjugated monomers.

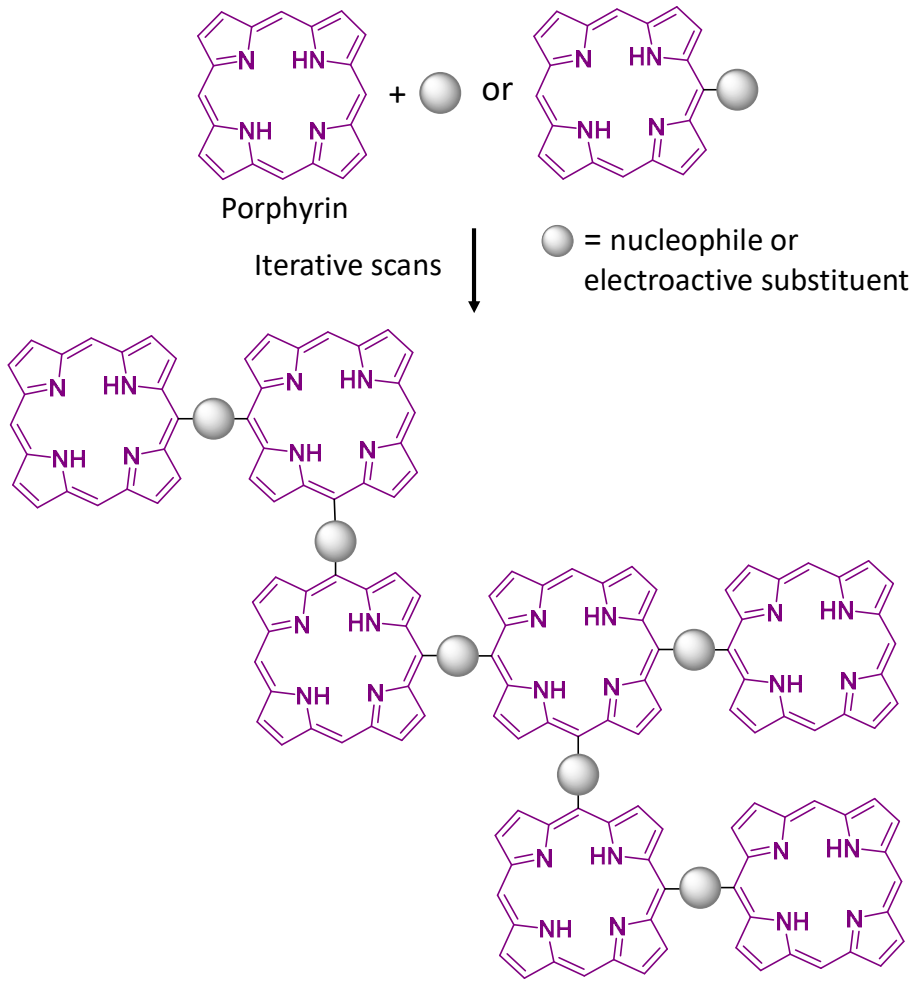

Figure 6. Porphyrins functionalized with electroactive substituents (right) can undergo direct self-electropolymerization or electrocopolymerization with other conjugated monomers. In the presence of a bridging nucleophile (left), these pathways lead to the formation of conjugated porphyrin-based polymer networks[83,84].

The electropolymerization of porphyrins can be traced back to the pioneering work of Macor and Spiro, who first reported the formation of stable porphyrin electrode films through the electrooxidation of metalloprotoporphyrins[81]. Subsequent studies expanded this concept toward electropolymerization pathways based on oxidative radical coupling through polymerizable substituents on the periphery of the porphyrin. In this approach, electrooxidation of the substituents generates radical species that initiate polymer growth either through substituent-substituent coupling or via electrophilic attack on meso or β positions of neighboring porphyrin units[81,85–89]. These mechanisms offer considerable flexibility in controlling

polymer architecture, conjugation pathways, and the resulting electronic properties of the polymer network.

Electropolymerization has been demonstrated for porphyrins bearing amine-, carbazole-, pyrrole-, hydroxy-, and thiophene-substituted phenyl groups, along with their derivatives[85–87,90–94]. In particular, porphyrins substituted at meso positions with aminophenyl groups were electropolymerized through a mechanism analogous to polyaniline formation, except that coupling occurs via electrophilic attack at ortho positions of adjacent aminophenyl groups, resulting in porphyrin units linked by dihydrophenazine (PzH_2) and/or phenazine (Pz) bridges (Figure 7)[95–98]. In a related approach, superoxide-assisted electrochemical polymerization has been reported for amino- and hydroxyphenyl-substituted porphyrins, where electrochemically generated superoxide species in dimethyl sulfoxide (DMSO) promote polymerization through these substituents[99–102]. Collectively, these studies demonstrate the feasibility of electropolymerizing porphyrins bearing electroactive substituents. These approaches provide significant flexibility in tailoring polymer architecture and conjugation pathways[81,103]. However, a key limitation of substituent-based electropolymerization is the need for prior synthetic functionalization of the porphyrin macrocycle, which increases synthetic complexity and restricts the use of commercially available porphyrins.

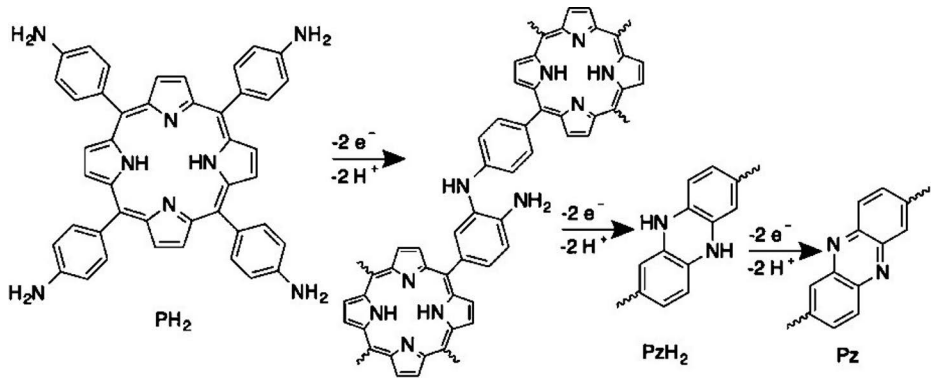

Figure 7. Proposed dimer structure of Poly(H_2TAPP), highlighting the formation of dihydrophenazine (PzH_2) and/or phenazine (Pz) inter-unit linkages[95,96].

To overcome this constraint, Ruhlmann and co-workers introduced a versatile electrocopolymerization strategy based on the use of external nucleophilic bridging agents. This method enables the direct electropolymerization of commercially available free-base or metalloporphyrins without requiring pre-functionalization. This approach significantly reduces synthetic complexity while retaining access to extended conjugated porphyrin-based polymer networks, although it requires careful

selection of both the porphyrin and the Lewis base used as the bridging spacer to ensure effective polymer formation[84].

This strategy uses the inherent reactivity of the porphyrin macrocycle under oxidative conditions, particularly at the methine bridge positions[83,84]. The mechanism relies on the generation of porphyrin dications at the second ring-oxidation potential, which exhibit enhanced electrophilic character and are therefore highly susceptible to nucleophilic attack. The distinction between these oxidation states is critical. While radical cations typically yield only monosubstituted products, dications provide sufficient activation for the sequential coupling reactions required for polymer growth[104–106]. This higher oxidation state facilitates the rapid formation of isoporphyrin intermediates, which subsequently propagate the polymerization process. In the presence of bifunctional nucleophiles (i.e., species possessing at least two spatially distinct reactive sites), multiple porphyrin units can be interconnected. The nucleophilicity and geometric arrangement of these sites influence both polymerization efficiency and the resulting film morphology. A key feature of this methodology is its versatility. Octaethylporphyrins are particularly suitable due to the favorable reactivity of their methine positions[107–111].

Thus, electrocopolymerization has emerged as an effective strategy for integrating porphyrins with other electroactive monomers to form conjugated hybrid polymer networks. For instance, Aguirre and co-workers demonstrated the simultaneous electrocopolymerization of metal-tetrakis(para-aminophenyl)porphyrins with aniline and its derivatives in aqueous media[112–114]. Similarly, thiophene-substituted porphyrins have been successfully electrocopolymerized with thiophene-based monomers. Porphyrins bearing 2-thienyl substituents were copolymerized with 3-methylthiophene and 3-hexylthiophene using electrochemical polymerization methods[115]. Furthermore, meso-tetrakis(thienyl)porphyrin monomers, either in their free base or complexed with Zn(II), have been electrocopolymerized with thiophene or 3,4-ethyleneldioxythiophene (EDOT) in boron trifluoride diethyl ether[103]. These studies highlight the versatility of electrocopolymerization in incorporating porphyrin units into conducting polymer frameworks, providing a powerful platform for designing multifunctional materials.

1.10 Porphyrin Electropolymers for Electrochromism

Porphyrin-based electrochromic polymers remain relatively underexplored despite their promising characteristics. Owing to their rich redox chemistry, extended π-conjugation, and tunable optical properties, porphyrins represent an attractive class of electrochromic building blocks. Their intense absorption in the visible region and ability to undergo multiple, reversible oxidation steps make them particularly well-suited for multicolor electrochromic applications. However, only a limited number

of porphyrin systems have been systematically studied with respect to their electrochromic performance, switching behavior, and long-term stability. Representative examples are summarized in Table 2.

Among the aminophenyl-substituted porphyrins, poly-5,10,15,20-tetrakis(4-aminophenyl)porphyrin (poly-H_2TAPP) films represent one of the most extensively studied systems. These films exhibit reversible electrochromic responses, switching from golden yellow to green, which gradually transitions to a reddish-brown and ultimately to black at higher positive oxidation potentials or upon exposure to APS. The color transitions can be driven either electrochemically or through chemical redox agents, demonstrating the versatility of the system[96]. Porphyrins bearing diphenylamine substituents constitute another promising class of EC materials. Electropolymerized films of both free-base and Pd(II) 5,10,15,20-tetrakis(4-*N,N*-diphenylaminophenyl)porphyrin display strong electrochromic properties with rich color palettes. In particular, the Pd(II) polymer exhibits multicolor switching through pale yellow, orange, green, and blue states upon oxidation, while maintaining excellent stability over more than 100 switching cycles. This combination of cycling stability and broad color range highlights the potential of metalloporphyrin systems for practical electrochromic devices[116].

Similarly, asymmetric porphyrin architectures based on free-base (H_2) and Zn(II) porphyrins functionalized with carbazole (CBZ) and triphenylamine (TPA) units have been successfully electropolymerized to yield films with reversible color switching. The Zn(II) derivative exhibited particularly distinct chromatic transitions, shifting from yellow in the neutral state through greenish intermediate states to a greenish-blue color upon full oxidation. This gradual color progression indicates the presence of multiple accessible redox states within the polymer matrix[94].

Thiophene-functionalized porphyrins have emerged as promising candidates for multielectrochromic applications, benefiting from the well-established electrochemical properties of polythiophene systems. For example, meso-tetrakis(thienyl)porphyrin Zn(II) derivatives, when electrocopolymerized with thiophene and 3,4-ethylenedioxythiophene (EDOT) in boron trifluoride diethyl ether (BFEE), form composite polymers displaying pronounced and reversible color changes. The incorporation of EDOT, known for enhancing conductivity and processability in conjugated polymers, likely contributes to the enhanced EC performance of these hybrid materials[103]. Related copolymer systems based on meso-tetrakis(2-thienyl)porphyrin, in both free-base (H_2Por) and Zn(II) (ZnPor) forms, have been prepared by electrocopolymerization with 3-methylthiophene (3MT) and 3-hexylthiophene (3HT). These films exhibit electrochromic switching centered around 600 nm, transitioning from pale yellow or transparent states to gray upon oxidation. Variation in the alkyl substituents on the thiophene comonomers

provides an effective strategy for tuning film morphology, solubility, and potentially the optical contrast of the electrochromic response[115].

Despite these encouraging advances, several challenges remain in the development of porphyrin-based electrochromic materials for practical applications. In addition to the relatively small number of systematically studied systems, several other reports merely claim electrochromic behavior, thereby limiting meaningful comparison between materials. Critical areas requiring further investigation include the optimization of switching speeds, the enhancement of optical contrast ratios, the improvement of long-term cycling stability, and the establishment of clear structure-property relationships linking porphyrin molecular design to electrochromic behavior.

Table 2. Comparison of electrochromic properties of electrocopolymerized porphyrin-based polymer films reported in the literature. Tb(s) is the time to reach 90 % of the bleached (oxidized) state, and Tc(s) is the time to reach 90 % of the colored (reduced) state, and *CE* is the chromic efficiency.

Polymer	Absorption peak (nm)	Optical Contrast	Tb(s) @ applied potential (V)	Tc(s) @ applied potential (V)	CE (cm^2C^{-1})	EC stability after 200 cycles (%)
P(2Por-co-Th)[103]	468	19	2.1 @ -0.4 V	2.9@ 1.0 V	132	78
P(2Por-co-EDOT)[103]	558	32	2.4 @ -0.6 V	3.3@ 0.8 v	178	93
P(3Por-co-EDOT)[103]	523	26	3.8 @ -0.8 V	1.2@ 0.8V	112	92
P(2Por(Zn)-co-Th)[103]	483	23	1.8 @ -0.4 V	2.3 @ 1.0 V	121	72
P(2Por(Zn)-co-EDOT)[103]	437	27	1.7 @ -0.6 V	1.9 @ 0.6 V	166	89
P(3Por(Zn)-co-Th)[103]	457	24	1.8 @ -0.6 V	1.9 @ 0.8 V	145	77
P(3Por(Zn)-co-EDOT)[103]	565	28	2.4 @ -0.8 V	2.2 @ 0.8 V	163	91
Por/3M[115]	600	2	-	-	-	-
Por/3HT[115]	600	29	-	-	-	-
ZnPor/3MT[115]	600	9.4	-	-	-	-
ZnPor/3HT[115]	600	11	-	-	-	-
Poly(ZnTAPP-EDOT)[II]	575	25	0.4 @-0.5V	0.7 @ 0.5 V	434	88
Poly(ZnTAPP-EDOT)[II]	1020	31	0.6 @-0.5 V	1.8 @ 0.5 V	182	83

1.11 Porphyrin Electropolymer for Supercapacitors

Electropolymerized porphyrins have emerged as a versatile class of pseudocapacitive materials for supercapacitor applications, combining the intrinsic redox activity of the porphyrin macrocycle with the structural advantages of conjugated polymer networks. Several electropolymerization strategies have been reported, including carbazole radical-cation coupling[117], vinyl/acetylene polymerization of chlorophyll and protoporphyrin derivatives[118,119], EDOT coupling in perfluorinated porphyrins[120], and vinyl polymerization of naturally abundant porphyrins, yielding diverse polymer architectures. The reported gravimetric capacitances span a wide range, from 31 to 466 F g^{-1}, with the highest values achieved in nickel-containing chlorophyll polymers[119], where the combination of small nanoparticle size, high conductivity, and additional metal-centered redox activity contribute synergistically to charge storage. Manganese protoporphyrin polymers also exhibit enhanced capacitance attributed to their multilayer lamellar structures and Mn-based redox transitions[118]. The analysis also reveals that high-performance porphyrin electropolymers are predominantly capacitive in nature, indicating efficient EDLC processes compared to diffusion-limited behavior. Electrochemical impedance spectroscopy further confirms low charge-transfer resistance across these systems.

Overall, these studies highlight that electropolymerization is an effective strategy to transform porphyrins into high-performance supercapacitor electrode materials, where the interplay between molecular redox chemistry, polymer growth mechanism, and nanoscale morphology governs charge storage behavior. Although the number of reported systems remains limited, these findings highlight the strong potential of porphyrin electropolymers as tunable and multifunctional materials for next-generation energy storage devices.

Table 3. Comparison of electrochemical supercapacitor performance of electropolymerized porphyrin-based materials.

Polymer	Polymerizable Groups	Electrolyte (Testing)	Potential Window (V)	Max Capacitance (Fg^{-1})	Cycle Stability
Poly(Zn-mTCPP)[117]	4 carbazole units (N-substituted)	CH_2Cl_2 / 0.1 M $TBAPF_6$	0.4-1.4 V	142 Fg^{-1} @ 5 Ag^{-1}	---
PolyZnChl-V[119]	1 vinyl group at C3	CH_2Cl_2 / 0.1 M $TBAPF_6$	0.1-0.75 V	31 Fg^{-1} (73 μFcm^{-2}) @ 5 mVs^{-1}	---
PolyZnChl-A[119]	1 acetylene group at C3	CH_2Cl_2 / 0.1 M $TBAPF_6$	0-1.1 V	90 Fg^{-1} (73.8μFcm^{-2}) @ 5 mVs^{-1}	---
PolyNiChl-V[119]	1 vinyl group at C3	CH_2Cl_2 / 0.1 M $TBAPF_6$	0.7-1.3 V	422 Fg^{-1} (771 μFcm^{-2}) @ 5 mVs^{-1}	---
PolyNiChl-A[119]	1 acetylene group at C3	CH_2Cl_2 / 0.1 M $TBAPF_6$	0.7-1.3 V	466 Fg^{-1} (1006 μFcm^{-2}) @ 5 mVs^{-1}	85% after 5000 cycles @ 1.5 Ag^{-1}
PEDOT-TPPF16[120]	4 EDOT (3,4-ethylenedioxythiophene) units	ACN / 0.1 M TBAP	0.2 to -1.0 V	140 Fg^{-1} (oxidation); 330 Fg^{-1} (reduction)@ 10 Ag^{-1}	---
PolyPor[120]	2 vinyl groups at β-positions	CH_2Cl_2 / 0.1 M $TBAPF_6$	0.3-0.9 V	93 Fg^{-1} (153.5 $mFcm^{-2}$) @ 1 Ag^{-1}	~100% after 2000 cycles @ 1 Ag^{-1}
PolyMnPor-100[120]	2 vinyl groups at β-positions	CH_2Cl_2 / 0.1 M $TBAPF_6$	0-0.8 V	135 Fg^{-1} (189 $mFcm^{-2}$) @1 Ag^{-1} and 108Fm^{-1} @ 2 Ag^{-1}	~100% after 2000 cycles @ 1 Ag^{-1}
PolyMnPor-200[120]	2 vinyl groups at β-positions	CH_2Cl_2 / 0.1 M $TBAPF_6$	0-0.8 V	250 Fg^{-1} @ 2 Ag^{-1}	---
PolyMnPor-300[120]	2 vinyl groups at β-positions	CH_2Cl_2 / 0.1 M $TBAPF_6$	0-0.8 V	166 Fg^{-1} @ 2 Ag^{-1}	---
PolyPPER-CBZ on GC[121]	Carbazole	ACN / 0.1 M TBAP	0-0.6 V	266 Fg^{-1} @ 5 Ag^{-1}	40% after 3000 cycles @ 5 Ag^{-1}
PolyPPER-CBZ on ITO[121]	Carbazole	ACN / 0.1 M TBAP	0-0.8 V	149 Fg^{-1} @ 5 Ag^{-1}	35% after 3000 cycles @ 5 Ag^{-1}
PolyPPER-TPA on GC[121]	Triphenylamine	ACN / 0.1 M TBAP	0-0.6 V	310 Fg^{-1} @ 5 Ag^{-1}	90% after 3000 cycles @ 5 Ag^{-1}
PolyPPER-TPA on ITO[121]	Triphenylamine	ACN / 0.1 M TBAP	0-0.8 V	220 Fg^{-1} @ 5 Ag^{-1}	80% after 3000 cycles @ 5 Ag^{-1}

1.12 Porphyrin Electropolymers for Electrochromic Supercapacitors

To date, there are only two reports on porphyrin electropolymers that exhibit bifunctional electrochromic pseudocapacitor behavior[122]. In the first report, a Zn(II) porphyrin dendrimer bearing eight carbazole termini was electropolymerized through dicarbazole coupling, forming a hyperbranched, sponge-like three-dimensional network exhibiting a specific capacitance of 277 F g^{-1} and multicolor electrochromism[122]. In the second report, the porphyrin core is systematically tuned by varying the central metal (free-base, Zn, Cu, and Co) within a structurally analogous carbazole/triphenylamine-functionalized framework. Although all polymers display similar multicolor electrochromic behavior, the Cu(II)-containing network delivers the highest capacitance (332 F g^{-1}), which is attributed to increased surface roughness and electrolyte accessibility[123]. A detailed comparison of the key structural features, electrochromic behavior, and supercapacitor performance of these systems is summarized in Table 4. Despite these promising results, only a limited number of porphyrin electropolymer systems have been explored to date, indicating that this field remains at an early stage and holds substantial potential for further molecular design, mechanistic understanding, and device-level optimization.

Table 4. Electrochromic supercapacitor parameters of electropolymerised porphyrin-based materials.

Parameter	**PD-film**[122]	**P-P**[123]	**P-PZn**[123]	**P-PCu**[123]	**P-PCo**[123]
MONOMER					
Porphyrin core metal	Zn(II)	Free-base (H_2)	Zn(II)	Cu(II)	Co(II)
Peripheral electroactive groups	CBZ via TPA branches	CBZ + TPA	CBZ + TPA	CBZ + TPA	CBZ + TPA
Linkage units in polymer	Dicarbazole (DCBZ)	DCBZ + TPB	DCBZ + TPB	DCBZ + TPB	DCBZ + TPB
ELECTROCHROMIC PROPERTIES					
Color states (neutral → fully oxidized)	LB*@ -0.2 V LO*@1.2 V G*@1.5 V B* @1.7 V	PY*→P* →G* →BG*	PY*→P* →G* →BG*	PY*@-0.2 V P* @ 0.7 V G* @ 1.0 V BG*@ 1.3 V	PY*@ -0.2 V P* @ 0.7 V G *@1.0 V BG*@ 1.3 V
Electrochromic reversibility	Fully reversible	Fully reversible	Fully reversible	Fully reversible	Fully reversible
SUPERCAPACITOR PERFORMANCE					
GCD measurement solvent/ electrolyte	ACN / 0.1 M $TBAPF_6$	ACN /0.1 M $TBAPF_6$	ACN / 0.1 M $TBAPF_6$	ACN / 0.1 M $TBAPF_6$	ACN / 0.1 M $TBAPF_6$
GCD configuration	3-electrode (ITO)	3-electrode (ITO)	3-electrode (ITO)	3-electrode (ITO)	3-electrode (ITO)
Max specific capacitance (F/g) & current density	277 Fg^{-1} @ 4.5 Ag^{-1}	283 Fg^{-1} @ 5 Ag^{-1}	276 Fg^{-1} @ 5 Ag^{-1}	332 Fg^{-1} @ 5 Ag^{-1}	272 Fg^{-1} @ 5 Ag^{-1}
Capacitance retention after 3000 GCD cycles (%)	~80%	69.2%	65.3%	75.0%	71.4%
Capacitance retention at high current density	70% @ 54.5 Ag^{-1}	74.6% @ 25 Ag^{-1}	64.3% @ 25 Ag^{-1}	78.7% @ 25 Ag^{-1}	74.5% @ 25 Ag^{-1}
Energy density (Wh k/g)	9.5 @ 4.5 Ag^{-1}, ΔV=0.5 V	11.8 @ 5 Ag^{-1}, ΔV=0.5 V	11.5 @ 5 Ag^{-1}, ΔV=0.5 V	13.4 @ 5 Ag^{-1}, ΔV=0.5 V	12.1 @ 5 Ag^{-1}, ΔV=0.5 V
Power density (kW k/g)	1.4 @ 4.5 Ag^{-1}	2.8 @ 5 Ag^{-1}	3.3 @ 5 Ag^{-1}	2.8 @ 5 Ag^{-1}	3.2@ 5 Ag^{-1}

*LB → light brown, LO→ light orange, G → green, B → blue, PY → pale yellow, P →pinkish, G → greenish, BG → bluish-green.

2 Materials and Methods

2.1 Materials

The porphyrins used in this work were either synthesized[124,125] or obtained from Porphyrin Labs and Porphyrin Systems. Other monomers were sourced from the commercial suppliers specified below. Unless otherwise stated, all reagents and solvents were of analytical grade and were used without further purification.

The monomers included 3,4-ethylenedioxythiophene (EDOT, TCI, 98%) and 4,4′-bipyridine (Alfa Aesar, 98%). Ferrocene (Aldrich, 99%) was employed as a redox reference compound, while tetrabutylammonium hexafluorophosphate ($TBAPF_6$, TCI, 98%) was used as the supporting electrolyte. Before use, $TBAPF_6$ was dried in a vacuum oven at 70 °C for 2 h. The organic solvents used included anhydrous acetonitrile (ACN, Sigma-Aldrich, 99.9%), dichloromethane (DCM, VWR Chemicals, 99.8%), and 1,2-dichloroethane (DCE, Alfa Aesar, 99%). All solvents were freshly distilled before use and stored over 4 Å molecular sieves in an argon-filled glove box to minimize moisture contamination. High-purity nitrogen (N_2), carbon dioxide (CO_2), and argon (Ar) were supplied by AGA-Finland.

Fluorine-doped tin oxide (FTO)-coated glass substrates (sheet resistance of approximately 8–10 Ωsq^{-1}) and 3 mm glassy carbon electrodes were employed as working electrodes. Before electropolymerization, the FTO substrates were cleaned by sequential ultrasonication in acetone, ethanol, and deionized water for 10 min each, followed by plasma treatment for 3 min to remove organic contaminants. A platinum wire was used as the counter electrode, and an Ag/AgCl electrode served as the quasi-reference electrode for all electrochemical measurements (calibrated against ferrocene/ferrocenium couple (Fc/Fc^+), E_{ref} =0.45 V in 0.1 M $TBAPF_6$ in acetonitrile).

2.2 Characterization Techniques

2.2.1 Spectroscopy

Optical and spectroscopic characterization of the monomers and electropolymerized films was carried out using multiple techniques. UV-Vis absorption spectra were

recorded using an Agilent Cary 60 spectrophotometer. Monomers measured in DCE solution, while films were analyzed on FTO-coated glass substrates using bare FTO as the reference. Color coordinates were calculated in the CIELAB (L*a*b*) space using the Cary WINUV software under D50 illumination (5000 K). FTIR spectra were obtained using a Bruker Vertex 70 spectrometer equipped with MCT or RT-DLaTGS detectors. ATR mode was used for monomer powders, while reflection mode was used for polymer films. Raman spectra were recorded using a Renishaw inVia confocal Raman microscope using a 532 nm laser and a CCD detector. XPS measurements were performed using PerkinElmer PHI 5400 and Thermo Scientific Nexsa spectrometers with Mg Kα and Al Kα radiation sources, respectively.

2.2.2 Microscopy

Surface morphology of polymer films deposited on FTO substrates was examined using a Thermo Scientific Apero S field-emission scanning electron microscope (FE-SEM) equipped with an Oxford Instruments Ultim Max 100 EDS detector. AFM measurements were carried out using Veeco diCaliber and Park Systems AFM instruments with silicon-tipped cantilevers operated in tapping and non-contact modes, respectively. Image processing and analysis were performed using WSxM 4.0 and XEI software.

2.2.3 Potentiostat/galvanostat workstation

An Autolab PGSTAT101 potentiostat (Metrohm Autolab) was used for electropolymerization and in situ spectroelectrochemical measurements. Supercapacitor performance was evaluated using cyclic voltammetry (CV), galvanostatic charge-discharge (GCD), electrochemical impedance spectroscopy (EIS), and long-term cycling stability measurements. These experimetns were conducted using an Ivium CompactStat potentiostat (Ivium Technologies), and a BioLogic VSP-300 multichannel potentiostat/galvanostat workstation (BioLogic Science Instruments).

2.3 Electropolymerization

Electropolymerization was carried out using a potentiostat/galvanostat in a three-electrode configuration. The electrolyte solution contained porphyrin and/or monomer dissolved in a mixed organic solvent (DCE: ACN = 4:1, v/v) with 0.1 M $TBAPF_6$ as the supporting electrolyte. Polymer films were electrodeposited on clean FTO substrates by cyclic voltammetry within an optimized potential window that enabled oxidation of both species while preventing overoxidation. Films were

prepared by applying 10, 20, or 25 potential cycles, depending on the intended characterization technique. After polymerization, the electrodes were rinsed thoroughly with the corresponding solvent to remove residual monomers and oligomers, dried, and stored in a desiccator. The electrochemical cell setup used for electropolymerization is illustrated in Figure 8.

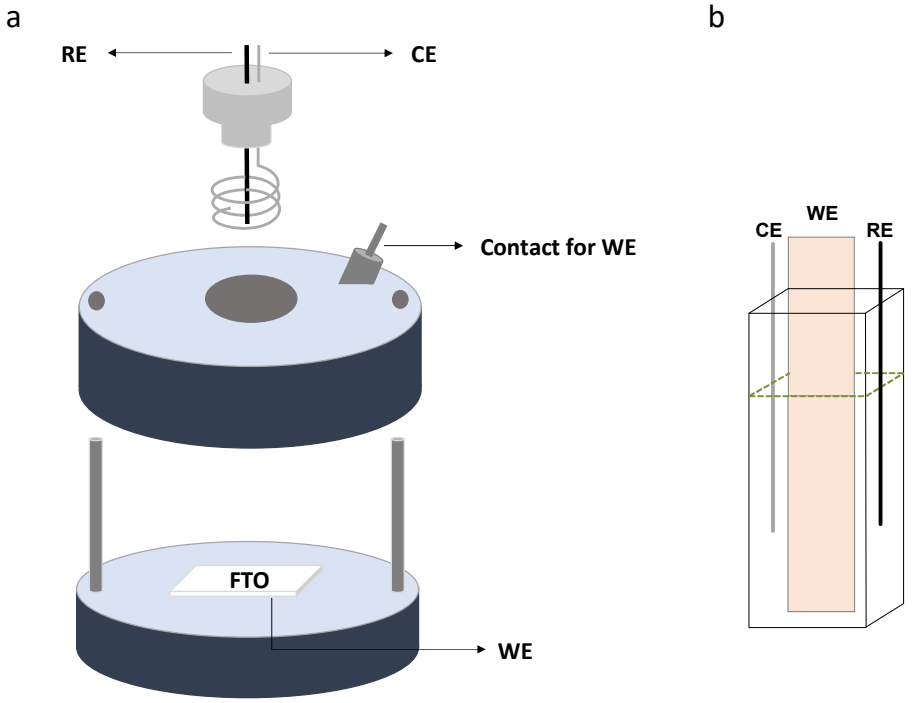

Figure 8. Three-electrode electrochemical cell setups used for electropolymerization. *[FTO is Fluorinated tin oxide, WE is working electrode, RE is reference electrode, and CE is counter electrode]*

2.4 Spectroelectrochemistry

2.4.1 In situ UV-Vis

In situ UV-Vis measurements were performed in a quartz cuvette (path length 1 cm) using an electrochemical cell consisting of FTO as the working electrode, a Pt wire as the counter electrode, and Ag/AgCl as the quasi-reference electrode. The cell was connected to an Autolab PGSTAT101 potentiostat, and spectral changes were recorded using an Agilent Cary 60 UV-Vis spectrophotometer, with blank FTO used as the background correction. Spectra were acquired across the selected potential

window using chronopotentiometry, with each potential held for 60 s before measurement (Figure 9a).

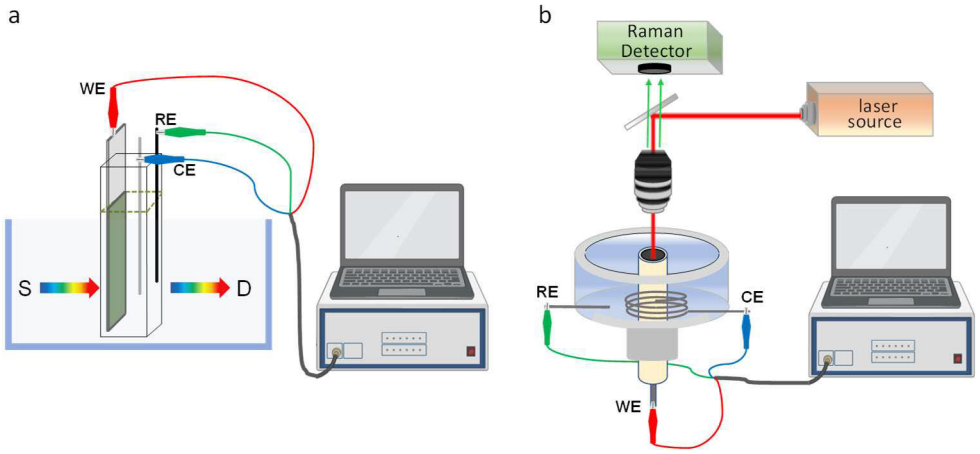

Figure 9. Schematic representation of the electrochemical cell setup used for (a) in situ UV-Vis and electrochromic measurements, and (b) in situ Raman measurements used in this study (S =source and D =detector).

2.4.2 In situ Raman

In situ Raman measurements were performed using a Renishaw inVia confocal Raman microscope equipped with a CCD detector and a Leica optical microscope. The electrochemical setup consisted of an FTO working electrode, a Pt wire counter electrode, and an Ag/AgCl quasi-reference electrode, all connected to an Autolab PGSTAT101 potentiostat. Diode lasers with wavelengths of 532, 633, and 785 nm were used as excitation sources. Measurements were performed using a 50× objective, with a laser operated at a power of 10 mW. A grating 1800 lines mm^{-1} grating was used for the 532 and 633 nm lasers (1200 lines mm^{-1} for 785 nm). Spectra were recorded at different applied potentials within the selected potential window under potentiostatic control (Figure 9b).

2.5 Electrochromic Measurements

Electrochromic measurements were performed in a quartz cuvette (path length, 1 cm) using an electrochemical cell comprising FTO as the working electrode, a Pt wire counter electrode, and an Ag/AgCl quasi-reference electrode. Polymer films (1.2 cm^2) deposited on FTO substrates served as the active working electrodes. The optimum potential range and corresponding color transitions were determined from

in situ UV-Vis measurements, which were used to define the potential window for electrochromic switching. The optical switching response was evaluated over 200 cycles at selected wavelengths within this potential range, with a switching interval of 20 s.

For optical memory (open-circuit) studies, the optical response of the polymer films was monitored at selected wavelengths as a function of time by alternating between the selected potentials for 2 s, followed by an open-circuit interval of 200 s.

2.6 Electrochemical characterization

All measurements were carried out at room temperature using three-electrode and/or symmetric two-electrode configurations (paper I). In a three-electrode setup, the electropolymerized porphyrin copolymer thin film on FTO-coated glass was used as the working electrode (WE), a platinum wire as the counter electrode (CE), and Ag/AgCl as the reference electrode (RE). For a symmetric two-electrode system, an identical electropolymerized porphyrin copolymer thin film on FTO-coated glass was used as WE and CE. 0.1M $TBAPF_6$ or 4 m $ZnCl_2$ were used as supporting electrolytes for electrochemical studies.

2.7 Computational Studies

Spin-restricted density functional theory (DFT) calculations were carried out using the Gaussian 16 software package. The electron exchange-correlation interactions were treated with the B3LYP hybrid functional. The LANL2DZ basis set was applied for Zn and Ni, while a 6-31G(d) basis was used for the lighter atoms (C, N, S, O, and H). For Zn, a valence configuration of $4s^2 3d^{10}$ was considered, whereas all electrons were included for the remaining elements. Empirical dispersion corrections were included using the GD3 scheme. For EDOT ligands, the same B3LYP functional and 6-31G(d) basis set was employed. The stability of all optimized geometries was verified through frequency calculations. Molecular orbitals were visualized using the VESTA software. Electronic absorption spectra were calculated using time-dependent DFT (TD-DFT) with both B3LYP and CAM-B3LYP hybrid functionals. The wavefunctions were expanded using the 6-311G(d) basis set for C, H, S, N, and O atoms, while LANL2DZ and GD3 dispersion corrections were retained for Ni and Zn (papers I &II).

To explore the polymerization behavior of keto-functionalized octaethylporphyrin (OEP) with 4,4′-bipyridine (4,4′-bpy), DFT calculations were performed to identify the most favorable meso-position for the initial nucleophilic attack. All four meso sites were optimized individually, and the most stable configuration was further examined by introducing a second 4,4′-bpy molecule to

evaluate the effect of the central metal ion. Calculations were carried out using the Kohn-Sham framework of DFT with the projector augmented wave (PAW) method and the Perdew-Burke-Ernzerhof (PBE) functional within the generalized gradient approximation (GGA), as implemented in VASP[126,127]. A cubic supercell with a vacuum spacing of 15 Å in all directions was used to eliminate intermolecular (periodic-image) interactions. Energy convergence was set to 10^{-4} eV, and atomic positions were relaxed until residual forces were below 0.01 eV $Å^{-1}$. Molecular structures were built in QuantumWise VNL 2017.1, and the optimized M-N bond lengths for ZnOEPK (2.05 Å) and NiOEPK (1.96 Å) showed excellent agreement with reported experimental data. The HOMO and LUMO orbitals were visualized with an isosurface level corresponding to one-tenth of the maximum electron density (paper III).

3 Results and Discussion

3.1 Electropolymerization of Porphyrins

Electropolymerization is one of the most efficient approaches for generating covalently bonded polymer films directly on electrode surfaces[128]. In this study, two different electropolymerization strategies for porphyrins were examined.

3.1.1 Electropolymerization via Electroactive Substituents

This work aimed to develop and investigate porphyrin-based electroactive polymer thin films derived from MTAPP (M = Zn^{2+}, Ni^{2+}, or H_2), both as homopolymers and as copolymers with EDOT, on conductive substrates. The influence of the central metal ion on the structural, morphological, electronic, and electrochromic properties of the thin films was examined. In situ UV-Vis and Raman spectroelectrochemical studies were conducted to elucidate the molecular-level mechanism of the electrochromic response. TD-DFT calculations were performed to provide additional insight into the electronic structure and optical properties of the copolymers. Finally, the dual electrochromic and supercapacitive performance of these materials were evaluated in a concentrated aqueous electrolyte to establish a structure-property relationship for porphyrin-based electroactive polymers in sustainable, water-based electrochemical systems.

Porphyrin homopolymers or copolymers were synthesized using electropolymerization techniques (papers I & II) in DCE:ACN (4:1, v/v) in 0.1 M $TBAPF_6$ on the FTO electrode surfaces. The potential was swept from 0.2 to 1.4 V *vs.* Ag/AgCl at a scan rate of 20 mV s^{-1}, using a monomer/s concentration of 0.04 mM. During electropolymerization, porphyrins bearing electroactive amino substituents at the meso position are first oxidized to generate radical cation intermediates, which subsequently undergo intermolecular coupling to form a conjugated polymeric network. Notably, the applied potential must be maintained below the oxidation potential of the porphyrin ring to preserve the π-conjugated macrocycle, which is essential for maintaining its intrinsic electronic structure[96,129]. In this work, MTAPP (M = Zn^{2+}, Ni^{2+}, or H_2) was successfully electropolymerized to form homopolymer thin films and electrocopolymerized with EDOT to obtain the corresponding copolymer thin films.

The electropolymerization mechanism of MTAPP is well established and proceeds analogously to that of aniline (Figure 7). However, unlike aniline, where polymerization occurs through para coupling, MTAPP polymerizes via the ortho position of the aminophenyl substituents, forming redox-active dihydrophenazine and phenazine linkages (papers I & II) [96,129].

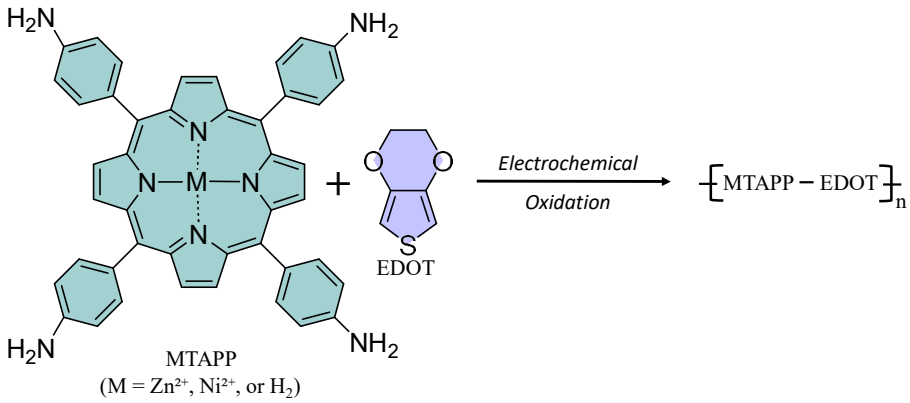

Scheme 1. Electrocopolymerization of MTAPP and EDOT in DCE:ACN (4:1) in 0.1 M $TBAPF_6$ on the FTO electrode surface. (Papers I & II).

In the case of MTAPP-EDOT electrocopolymerization (Scheme 1), the process is initiated by the oxidation of the amino substituents on MTAPP and the C_α position of EDOT units, generating corresponding radical cations that subsequently undergo intermolecular coupling to form an extended conjugated copolymer network. The gradual increase in current observed in successive cyclic voltammetry scans confirms progressive film growth, resulting in uniform, adherent, and electroactive copolymer film on the electrode surface (Figure 10a,d,g). The formation of homogeneous, brightly colored thin films on the electrode surface further confirms successful polymer deposition (Image 1).

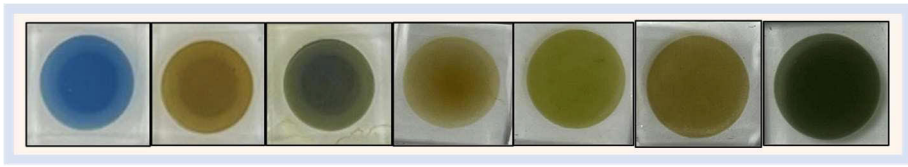

Image 1. From Right to left, PEDOT, poly(ZnTAPP), poly(ZnTAPP-EDOT), poly(H_2TAPP), poly(H_2TAPP-EDOT), poly(NiTAPP), and poly(NiTAPP-EDOT) were electropolymerized in 0.1 M $TBAPF_6$/ACN on the FTO electrode surface.

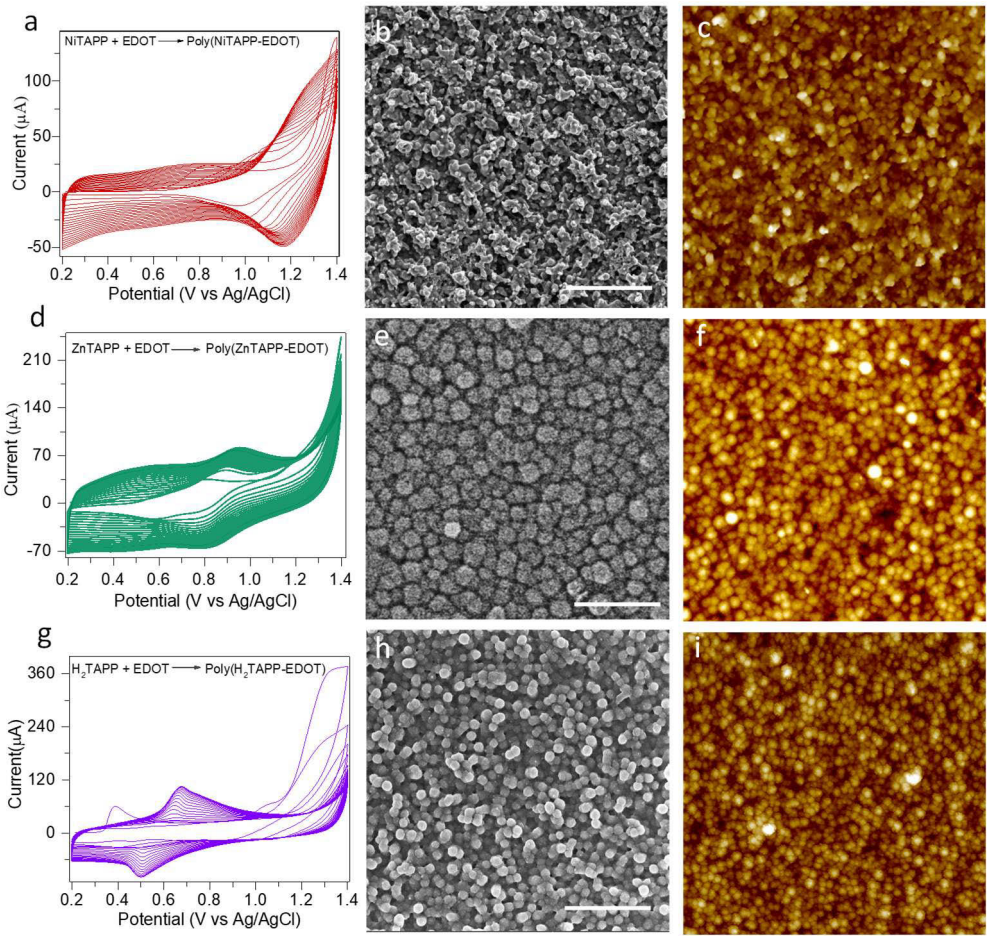

Figure 10. (a, d, g) CVs of electrocopolymerization of poly(NiTAPP-EDOT), poly(ZnTAPP-EDOT), and poly(H_2TAPP-EDOT) in DCE:ACN (4:1) in 0.1 M $TBAPF_6$ on the FTO electrode surface, respectively, (b, e, h) corresponding SEM images (scale- 1μm), and (c, f, i) AFM images (scale- 5μm x5 μm) of the respective copolymer thin films (papers I & II).

3.1.2 Electropolymerization via Bridging Ligands.

The objective of this work was to electropolymerize keto-functionalized octaethylporphyrins (MOEPK; M = Zn^{2+}, Ni^{2+}) using 4,4′-bpy as a bifunctional bridging nucleophile, thereby enabling direct polymer film formation without prior monomer functionalization. The influence of the central metal ion and keto functionalization on the electropolymerization mechanism and resulting polymer architecture was investigated, and DFT calculations were performed to provide insight into the growth behavior and the role of the metal center.

The electropolymerization strategy involves the use of suitable bridging ligands (nucleophiles), as originally described by Ruhlmann et al[83,84]. In this approach

(scheme 2), the bridging ligands, which act as Lewis bases, must contain at least two accessible nucleophilic sites in their structures to enable polymer formation (paper III). Electropolymerization is initiated by oxidation of the porphyrin macrocycle to its dicationic form, generating electrophilic centers at the meso positions. In metalloporphyrins, polymer film formation does not occur if the applied potential is limited to oxidation of the central metal ion; instead, it is governed by oxidation of the porphyrin macrocycle [83,84].

In the electropolymerization of Zn and Ni keto-octaethylporphyrins (MOEPK), anodic oxidation generates dication species that readily undergo nucleophilic addition with 4,4′-bpy. The process was carried out in a solution containing MOEPK (2.5 mM) and 4,4′-bpy (2.5 mM) in 0.1 M $TBAPF_6$ dissolved in DCE:ACN (4:1 v/v). Cyclic voltammetry was performed for 25 cycles at a scan rate of 200 mV s^{-1} over the potential range of -0.55 to 1.55 V for NiOEPK and -0.6 to 1.6 V for ZnOEPK. Typically, three oxidation peaks are observed during the electropolymerization process. The first two correspond to the formation of cationic and dicationic species, while the third is attributed to the oxidation of the isoporphyrin intermediates. As cycling proceeds, these features shift towards more positive potentials and gradually merge into a broader signal. Furthermore, an increase in current indicates continuous polymer thin film growth on the electrode surface (Figure 11a,b). Since four meso positions (5, 10, 15, and 20) are available in MOEPK, coupling may occur at different positions, leading to either linear or branched architectures. Density functional theory (DFT) calculations were performed to understand the growth behavior and the role of different metal centers (paper III).

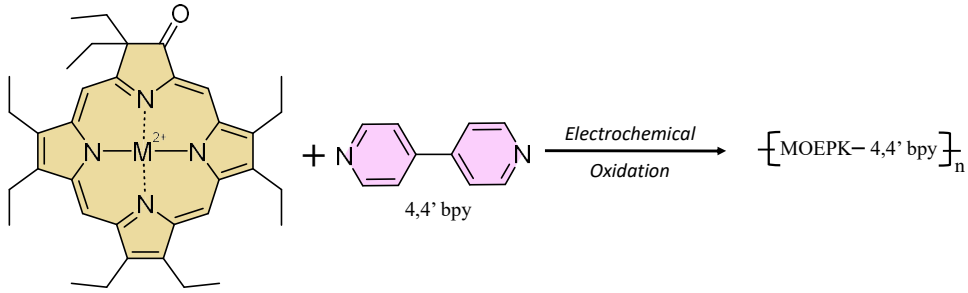

Scheme 2. Electropolymerization of MEOPK and 4,4′-bpy in DCE: ACN (4:1) in 0.1M $TBAPF_6$ with FTO as the working electrode

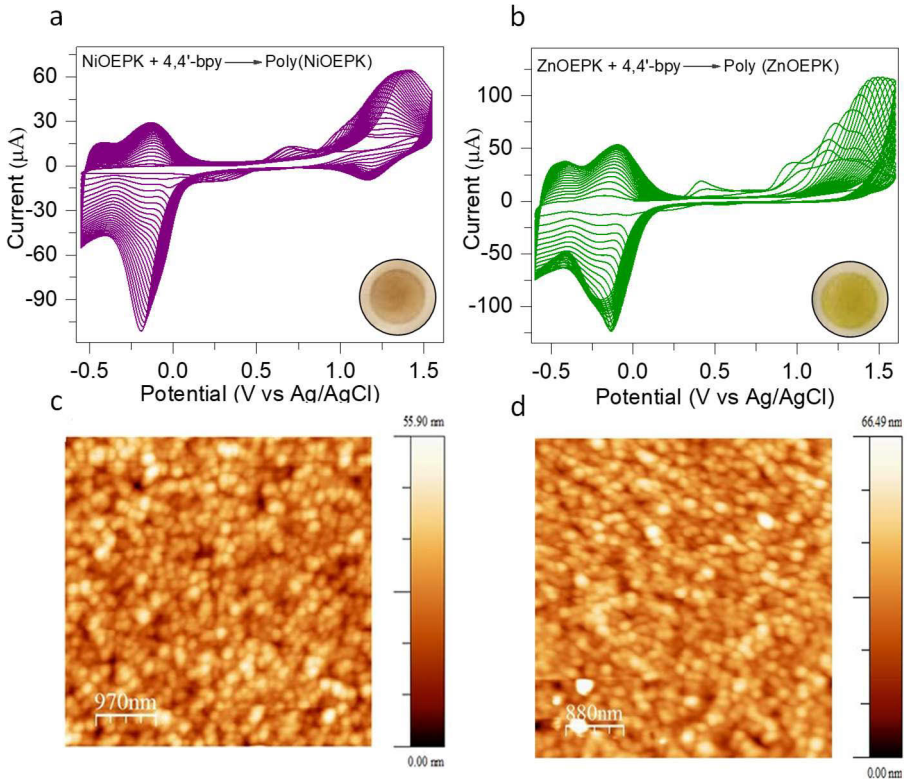

Figure 11. (a-b) Electropolymerization of MOEPK and 4,4′-bpy in DCE:ACN (4:1) in 0.1 M $TBAPF_6$ on FTO electrode surface and (c-d) AFM images (paper III). Inset a and b show the color of the polymer thin films.

3.2 Characterizations of Thin Films

UV-Vis spectroscopy was employed to investigate the optical properties of the porphyrin-based systems and to analyze the combined effects of polymerization and metal coordination on the electronic structure of the thin films. Porphyrins are chromophores with characteristic absorption features, including an intense Soret (B) band, and a series of lower-energy Q bands, owing to their highly conjugated π-electron systems. These features serve as reliable spectroscopic fingerprints for identifying porphyrin structures[130].

As summarized in Table 5, all porphyrin systems exhibited a prominent Soret band, confirming the presence and preservation of the porphyrin macrocycle. Generally, polyporphyrins exhibit a red shift and noticeable broadening of the Soret band compared to their monomeric counterparts. This behavior can be attributed to increased π-π stacking interactions and enhanced electronic delocalization between neighboring porphyrin units within the polymer backbone, indicating extended conjugation throughout the polymeric structure[131]. In the visible region, characteristic

Q-bands are observed for all systems; however, the number and spectral distribution depend on both the metal center and the nature of the polymer. Metal-free porphyrin systems display multiple Q bands, reflecting the lower symmetry of the free-base porphyrin core. In contrast, metallated porphyrin systems generally exhibit fewer Q bands due to increased molecular symmetry introduced by metal coordination (Figure 12 and paper III). These trends are maintained upon polymerization, although the polymeric materials tend to show broader and slightly red-shifted Q-band features. For porphyrin-EDOT copolymers, the Q bands extend further into the visible and beginning of near-infrared (bNIR) regions compared to their respective monomers. This extension suggests enhanced electronic communication along the polymer chain and partial band-gap narrowing as a result of increased conjugation (Figure 12). Additionally, the incorporation of EDOT units further modulates the absorption profile, indicating strong electronic interaction between the porphyrin core and the conducting polymer segments.

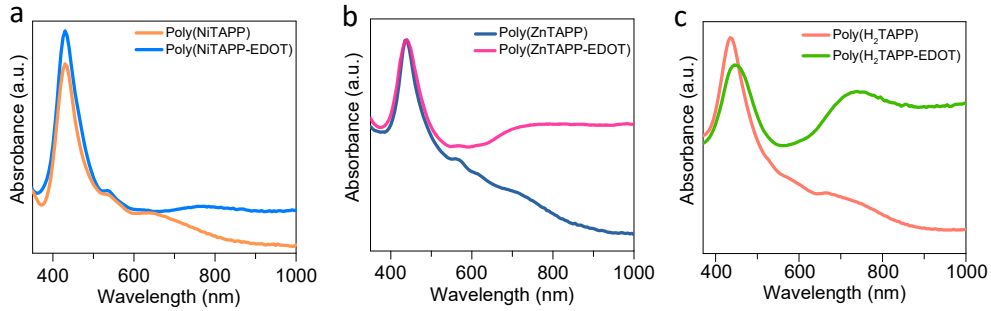

Figure 12. UV-Vis spectra of (a) poly(NiTAPP-EDOT) and poly(NiTAPP) (b) poly(ZnTAPP-EDOT) and poly(ZnTAPP), and (c) poly(H_2TAPP-EDOT) and poly(H_2TAPP).

SEM revealed the distinct morphological features of polymer thin films. PEDOT exhibited an interconnected network of nanofibers (average diameter 24 nm), whereas poly(MTAPP) formed compact globular structures. In contrast, poly(ZnTAPP-EDOT), poly(NiTAPP-EDOT), and poly(H_2TAPP-EDOT) displayed more complex morphologies, including flower-like architecture (~207 nm), porous granular structure composed of irregular cauliflower-like aggregates (~70-100 nm), a uniform nanogranular surface morphology composed of closely packed, quasi-spherical particles (~100-105 nm), respectively (Figure 10b,e,h). These morphological variations highlight the critical role of metal coordination in directing copolymer growth, nucleation behaviour, and film organization. The keto-functionalized porphyrin copolymers, poly(NiOEPK-4,4'-bpy) and poly(ZnOEPK-4,4'-bpy), displayed tightly packed, distorted spherical structures (Figure 11c,d). The observed porosity and surface textures facilitate ion diffusion during electrochemical processes, thereby enhancing electrochemical performance. EDX elemental mapping confirmed

a uniform distribution of elements (Ni/Zn, N, C, O, S) throughout the films, confirming homogeneous copolymer formation (papers I, II, & III).

FTIR, Raman, and XPS analyses were performed to characterize the chemical structure, bonding environment, and surface composition of copolymer thin films (papers I, II, & III). In FTIR spectra of poly(MTAPP), characteristic vibrational modes associated with the pyrrole ring, skeletal framework, ring deformations, and metal-nitrogen (Zn-N and Ni-N) bonds were clearly identified[132]. A weak band around 820 cm^{-1} was attributed to the amino groups coupling in poly(MTAPP), while the band at 1427 cm^{-1} supported the formation of phenazine linkages. Suggesting the coexistence of hydrazine and phenazine linkages within the polymer backbone[96,129]. In contrast, phenazine linkages were absent in poly(MTAPP-EDOT). Instead, characteristic bands corresponding to C-S-C stretching and alkylenedioxy group vibrations confirmed successful copolymer formation.

Raman spectroscopy complemented the FTIR results by providing well-defined vibrational features for both poly(MTAPP) and poly(MTAPP-EDOT). In the copolymers, the intense band at 1431 cm^{-1} was assigned to symmetric $C_\alpha=C_\beta$ stretching, while bands at 1512 and 1557 cm^{-1} were attributed to asymmetric $C_\alpha=C_\beta$ vibrations[132,133]. Additional Raman bands corresponding to symmetric C-S-C deformation, C-O-C deformation, and C_α-C_α inter-ring stretching further confirmed the incorporation of EDOT units into the polymer backbone (papers I & II). For poly(MOEPK), FTIR spectra confirmed the presence of C=O stretching from the five-membered strained ring at 1722 cm^{-1} and characteristic C=N stretching associated with the pyridinium moiety at 1620 cm^{-1}, along with additional vibrational modes originating from the porphyrin framework. Raman spectra displayed skeletal vibrations characteristic of the porphyrin core[134]. Notably, electropolymerization resulted in red-shifting and broadening of several characteristic bands in both FTIR and Raman spectra, leading to partial peak overlap. These spectral changes are consistent with increased conjugation and electronic delocalization within the polymer network (paper III).

XPS analysis confirmed the elemental composition and chemical states of the polymerized thin films. The C 1s spectrum was deconvoluted into multiple components corresponding to C-C/C=C, C-N, C=O, and C-S (When EDOT was used). The N 1s spectra provided crucial evidence for successful polymerization. For poly(MTAPP-EDOT), the S 2p region exhibited a characteristic spin-orbit doublet (1.2 eV separation), confirming the presence of thiophene sulfur from EDOT units[135]. Metal core-level spectra (Zn 2p and Ni 2p) confirmed the presence and chemical integrity of the metalloporphyrin centers[134]. The shake-up satellite features observed in the Ni spectra are consistent with Ni(II) in a porphyrin coordination environment, indicating preservation of the metalloporphyrin core during electropolymerization[134]. Overall, the XPS results strongly corroborate the structural conclusions drawn from FTIR and Raman spectroscopy (papers I, II & III).

Table 5. Summary of UV-Vis absorption bands of porphyrin monomers, homopolymers, and copolymers.

Material	Soret band (nm)	Q bands (nm)
NiTAPP (in DCE)	420	530
Poly(NiTAPP)	430	535
Poly(NiTAPP-EDOT)	430	535
ZnTAPP (in DCE)	430	555 & 600
Poly(ZnTAPP)	435	565 & 615
Poly(ZnTAPP-EDOT)	440	570
H_2TAPP (in DCE)	430	525, 565, 595 & 660
Poly(H_2TAPP)	435	570 & 665
Poly(H_2TAPP-EDOT)	445	-
NiOEPK (in DCM)	410	505, 545, 570 & 615
Poly(NiOEPK)	435	650
ZnOEPK (in DCM)	415	520,570 & 620
Poly(ZnOEPK)	440	655

3.3 In situ Studies

In situ UV-Vis and Raman spectroelectrochemical measurements were performed to monitor the redox-induced changes in the polymer thin films in both organic and aqueous media. In 0.1 M $TBAPF_6$/ACN, measurements were performed for all polymer films, and the influence of laser power on the Raman spectra was also evaluated. In aqueous 4 m $ZnCl_2$, analogous measurements were conducted for poly(NiTAPP-EDOT), PEDOT, and poly(NiTAPP)[136].

3.3.1 In Situ UV-Vis and Raman of polymer thin films in 0.1 M $TBAPF_6$/ACN

3.3.1.1 In Situ UV-Vis in 0.1 M $TBAPF_6$/ACN

In situ UV-Vis-bNIR spectroscopy enables real-time monitoring of chemical and electronic changes during electrochemical processes[136]. Here, in situ UV-vis

spectroelectrochemical measurements were performed in 0.1 M $TBAPF_6$/ACN solution (Figure 13). The poly(MTAPP) thin films did not exhibit significant spectral change across the applied potential range, indicating non-electrochromic behavior (Figure 13a,c,e). In contrast, poly(MTAPP-EDOT) thin films displayed pronounced and dynamic optical changes dominated by π-π* transitions upon electrochemical cycling, demonstrating the critical role of the EDOT unit. At -0.5 V, the copolymers exhibited a broadened Soret band, characteristic porphyrin Q band absorptions, and a feature band centered at 575 nm (Figure 13b,d,f). The band at 575 nm originates primarily from the π–π* transition of the EDOT backbone. This band gradually decreased upon oxidation, indicating depletion of neutral-state absorption and progressive oxidative doping of the EDOT backbone[137,138]. Throughout this process, the persistence of the Soret band confirms the structural integrity of the porphyrin macrocycle; however, a minor modulation in its intensity likely arises from changes in the local electronic environment induced by EDOT doping rather than direct porphyrin-centered redox chemistry. Concomitantly, a broad absorption band developed in the 700-800 nm region and intensified with increasing potential, characteristic of polaron formation within the conjugated polymer backbone. The presence of a well-defined isosbestic point indicates clean and reversible interconversion between neutral and doped electronic states. At higher oxidation potentials, an additional absorption band emerged beyond 900 nm, consistent with the formation of bipolaronic species within the EDOT segments[137,138]. Importantly, the electrochromic response was fully reversible, with the original spectral features completely restored upon returning to lower potentials, demonstrating highly reversible electrochemical doping/dedoping and excellent optical and electrochemical stability of the films. Together, these observations demonstrate that incorporation of EDOT enables efficient electrochemical doping and stabilization of charge-carrier states, resulting in a significantly enhanced electrochromic response in the copolymer compared to the corresponding porphyrin homopolymer.

For most polyconjugated systems, the position of Raman bands associated with the π-bonding is sensitive to the choice of excitation wavelength, whereas their relative intensities are an intrinsic property[138,139].

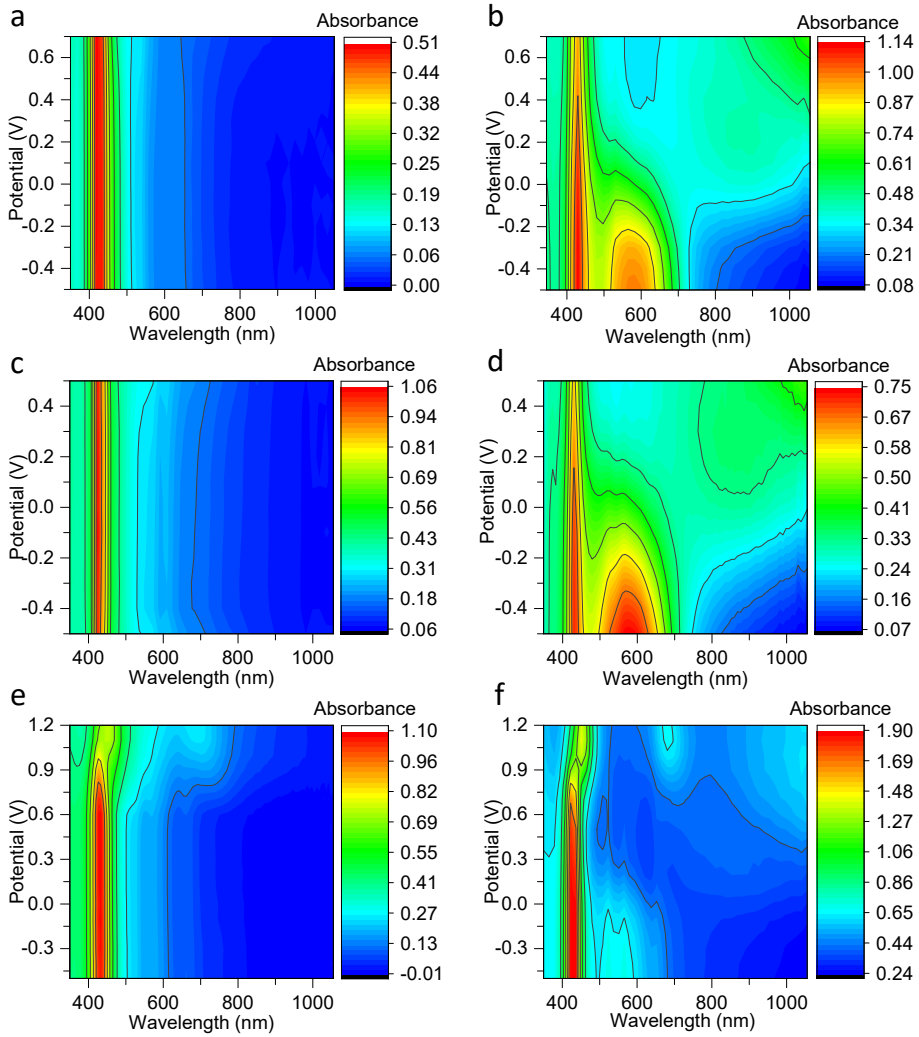

Figure 13. In situ UV-vis contour plots (a) poly(NiTAPP), (b) poly(NiTAPP-EDOT), (c) poly(ZnTAPP), (d) poly(ZnTAPP-EDOT), (e) poly(H_2TAPP), and (f) poly(H_2TAPP-EDOT) in DCE:ACN (4:1) in 0.1 M $TBAPF_6$ on FTO electrode surface

3.3.1.2 In Situ Raman in 0.1 M $TBAPF_6$ /ACN

In the Raman spectrum of poly(ZnTAPP-EDOT), several characteristic bands are observed (Figure 14a, $\lambda_{exc.}$=785nm). The most prominent feature is the symmetric C_α-C_β stretching deformation appearing at 1421 cm^{-1}, which is highly sensitive to the excitation wavelength. Additional ring skeletal features include the asymmetric C_α-C_β vibration at 1512 cm^{-1}, the C_β-C_β stretching at 1369 cm^{-1}, and the C-S-C ring deformation at 697 cm^{-1}. Bands at 1271 cm^{-1} and 1223 cm^{-1} are attributed to inter-ring C_α-$C_{\alpha'}$ symmetric stretching and C_β-H bending, respectively[138–141]. Upon increasing

electrode polarization, the symmetric C_α-C_β stretching mode exhibits a blue shift, whereas the asymmetric C_α-C_β mode shows a red shift. The positions of the remaining peaks remain largely unchanged; however, a gradual decrease in intensity indicates a reduction in the population of neutral (undoped) chain segments due to progressive electrochemical[138].

The choice of excitation wavelength plays a critical role in Raman spectroelectrochemical studies due to resonance enhancement effects associated with electronic transitions in the polymer thin films (Figure 14b). The green excitation line ($\lambda_{exc.}$= 532 nm) lies close to π-π* absorption maximum at 575 nm and selectively enhances vibrations from undoped PEDOT segments of poly(ZnTAPP-EDOT). The red line ($\lambda_{exc.}$= 632 nm), located near the tail of the neutral polymer absorption, produces similar behavior, resulting in a modest (3.7 cm^{-1}) red shift of the symmetric C_α-C_β stretching band (1431.6 cm^{-1}). The most informative spectra are obtained with $\lambda_{exc.}$=785 nm, which is close to the isosbestic point observed in the in situ UV-Vis spectra. Under this condition, a more pronounced redshift (11 cm^{-1}), accompanied by significant band broadening, is observed, indicating substantial doping-induced structural reorganization of the conjugated backbone.

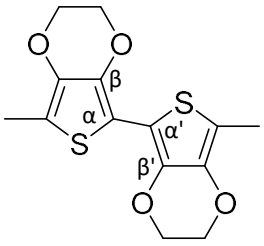

EDOT dimer

The influence of structural regularity on conjugation length can be understood by comparing the Raman characteristics of regioregular PEDOT with poly(ZnTAPP-EDOT). Across the excitation range from 532 nm to 785 nm, the symmetric C_α=C_β peak position shifts by only 4.5 cm^{-1}in PEDOT, reflecting a uniform conjugation. In contrast, in poly(ZnTAPP-EDOT), the peak shifts by 11 cm^{-1}, indicating a broader distribution of conjugation lengths arising from its structurally homogeneous polymer films. Similar trends were observed for other copolymers. Overall, structural regularity promotes extended and more uniform conjugation in polymer thin films, consistent with the previous reports[138–141].

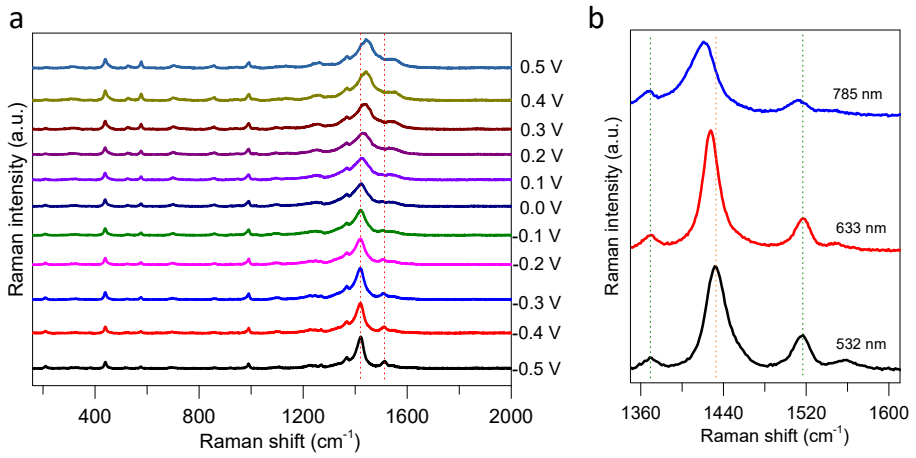

Figure 14. (a) Potential-dependent Raman spectrum of poly(ZnTAPP-EDOT) recorded at 785 nm excitation in 0.1 M $TBAPF_6$/ACN, with applied potentials from -0.5 V to +0.5 V vs. Ag/AgCl, and (b) Dependence of the symmetric (C_α=C_β) stretching frequency on excitation wavelength, illustrating the sensitivity of the EDOT backbone vibration to the energy of the incident laser.

3.3.2 In Situ UV-Vis and Raman of polymer thin films in aqueous 4 m $ZnCl_2$

3.3.2.1 In Situ UV-Vis in aqueous 4 m $ZnCl_2$

In situ UV-Vis spectroelectrochemistry of poly(NiTAPP-EDOT) in aqueous 4 m $ZnCl_2$ (Figure 15a) showed similar spectral features to those of 0.1 M $TBAPF_6$/ACN. At -0.5 V (neutral state), the spectrum is dominated by a Soret band at 430 nm, characteristic of the NiTAPP porphyrin core, alongside an absorption band at 560 nm attributed to the π-π* transition of the EDOT-containing conjugated backbone, and a Q-band at 535 nm. Upon a gradual increase in potential, the 560 nm absorption peak decreases continuously until +0.1 V and remains constant thereafter, consistent with the Raman results. Concurrently, a broad absorption band appears above 900 nm, indicating the formation of bipolaronic charge carriers within the conjugated backbone. At the same time, the Soret band at 430 nm undergoes a steady decrease in intensity with increasing potential, reflecting perturbation of the porphyrin electronic environment induced by oxidative doping of the EDOT segments. These trends are shown in Figure 15b. Importantly, all these spectral features were fully restored upon reversing the applied potential, confirming complete electrochemical reversibility of the doping-dedoping process across the investigated potential window (paper I).

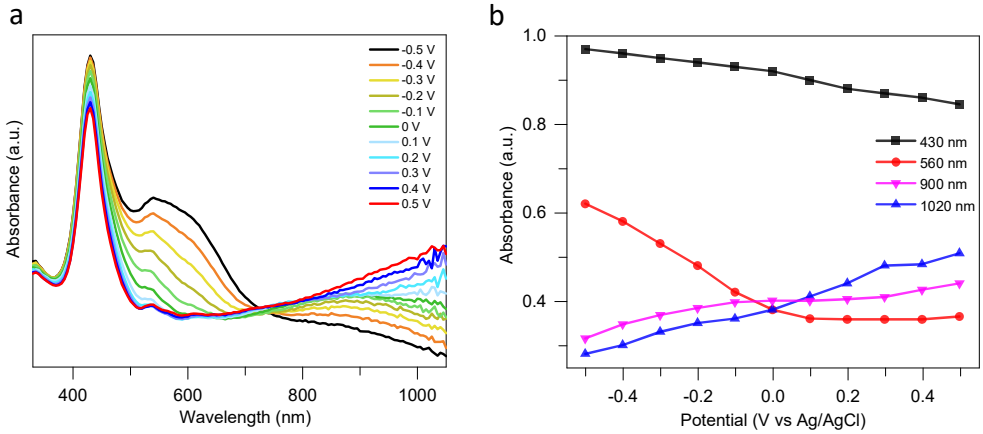

Figure 15. (a) In situ UV-Vis absorption spectrum of poly(ZnTAPP-EDOT) recorded in aqueous 4 M $ZnCl_2$ as a function of applied potential (-0.5 V to +0.5 V vs. Ag/AgCl) and (b) Potential-dependent absorbance study at 430 nm (Soret band), 560 nm (π–π* backbone transition), 900(polaron band), and 1020 nm (bipolaronic absorption band).

3.3.2.2 In Situ Raman in aqueous 4 m $ZnCl_2$

In situ Raman spectra of PEDOT, poly(NiTAPP-EDOT), and poly(NiTAPP) thin films were recorded using 532 nm excitation over an applied potential window from -0.5 to +0.5 V in aqueous 4 m $ZnCl_2$ electrolyte (Figure 16). The excitation wavelength overlaps with strong electronic transitions of both the NiTAPP chromophore (Soret and Q bands) and the undoped EDOT segments (π–π* transition), resulting in resonance enhancement of Raman modes associated with the neutral conjugated framework at low applied potentials. Consequently, spectra collected at negative potentials contain contributions from both EDOT backbone vibrations and NiTAPP core modes. A weak band observed at ~286 cm^{-1} originates from the $ZnCl_2$ electrolyte[142].

The electrochemical behavior of the PEDOT thin film has been extensively characterized through in situ Raman spectroelectrochemical studies[138,140,141], which clearly document the progression from neutral polymer to polaron and bipolaron states upon oxidation, and similar trends are also observed in 4 m $ZnCl_2$. Most spectral changes occur between 1200-1600 cm^{-1} region, where the principal vibrational modes of the thiophene-based backbone are active (Figure 16a). These include the symmetric C_α=C_β stretch at 1433 cm^{-1}, the asymmetric C_α=C_β stretch at 1518 cm^{-1}, the C_β-$C_{\beta'}$ deformation at 1370 cm^{-1}, and the inter-ring C_α-$C_{\alpha'}$ mode at 1268 cm^{-1} [138]. In the neutral state (-0.5 V), PEDOT exhibits an intense, sharp band at 1433 cm^{-1}, indicative of extended conjugation length. Upon oxidation, this band shifts to 1461 cm^{-1} with a concurrent decrease in intensity, attributed to diminishing resonance enhancement effect as the neutral polymer is progressively oxidized and charge carriers are introduced. The asymmetric C_α=C_β mode shows the opposite trend, shifting from 1519 cm^{-1} (at -0.5 V) to 1514 cm^{-1} (at -0.2 V) and remaining constant at more positive potentials (Figure 17)[140,141]. In contrast, porphyrin core vibrations of NiTAPP exhibit

only minor shifts in peak position, indicating that the macrocyclic framework remains largely unaffected by the applied potential[132,133]. Furthermore, no new Raman features indicative of irreversible chemical modification were observed across the entire potential window (Figure 16c). This behavior is fully consistent with the potential-dependent absorption changes observed in the corresponding in situ UV-Vis spectra.

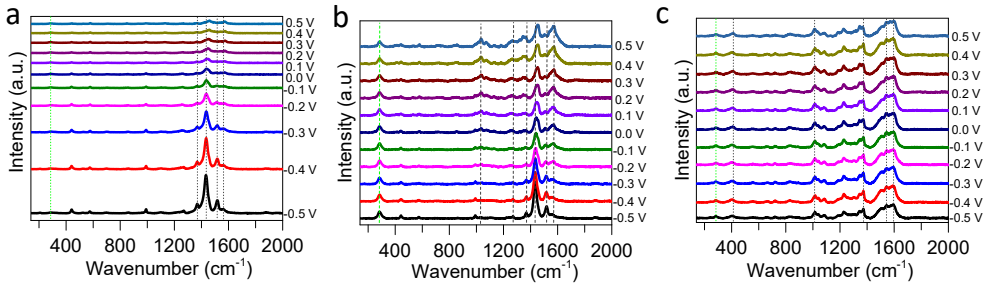

Figure 16. In situ Raman of (a) PEDOT, (b) poly(NiTAPP-EDOT), and (c) poly(NiTAPP) recorded at 532 nm excitation in aqueous 4 m $ZnCl_2$ as a function of applied potential (-0.5 V to +0.5 V vs Ag/AgCl).

For poly(NiTAPP-EDOT) thin film, the application of potentials induces systematic changes in the 1400-1600 cm^{-1} Raman region, mainly originating from the EDOT backbone (Figure 16b). Notably, the symmetric $\nu(C_\alpha{=}C_\beta)$ mode gradually shifts from ~1433 cm^{-1} at -0.5 V to ~1437 cm^{-1} at -0.2 V. This shift is observed when redox features begin to appear in the corresponding cyclic voltammogram. Furthermore, the shift reaches ~1453 cm^{-1} at +0.3 V and remains unchanged. This shift reflects increased quinoid characteristics and enhanced charge delocalization along the conjugated backbone. Concurrently, the asymmetric $\nu(C_\alpha{=}C_\beta)$ mode, initially centered at ~1517 cm^{-1}, shifts toward lower wavenumbers (~1500 cm^{-1}) until 0 V and remains unchanged thereafter, consistent with doping-induced structural reorganization of the EDOT segments and the emergence of polaronic and bipolaronic charge carriers (Figure 17)[140,141]. At higher positive potentials, these changes are accompanied by the growth of a pronounced tail extending to ~1574 cm^{-1}. This arises from increasing spectral overlap between the EDOT backbone and porphyrin-associated vibrations of NiTAPP, which become more prominent at higher doping levels[138]. Consequently, the symmetric $\nu(C_\alpha{=}C_\beta)$ band intensity also grows at higher potentials; however, this enhancement arises primarily from overlapping Raman peaks rather than the intrinsic intensity changes of the EDOT vibrational modes (paper I). In the cases of poly(ZnTAPP-EDOT) and poly(H_2TAPP-EDOT) thin films, a similar response in the Raman measurements indicates that the potential-dependent behavior is primarily dictated by the EDOT backbone and is largely insensitive to the porphyrin metal center.

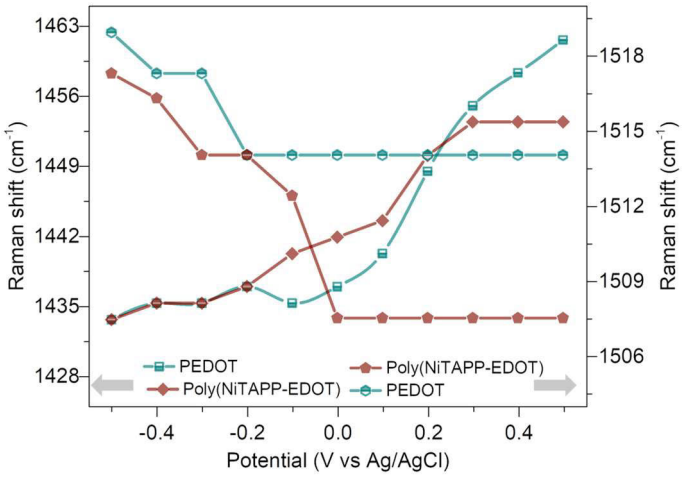

Figure 17. Raman band positions of the symmetric $\nu(C_\alpha=C_\beta)$ [1431-1463 cm^{-1}] and asymmetric $\nu(C_\alpha=C_\beta)$ [1507-1520 cm^{-1}] stretching modes at 532 nm for PEDOT and poly(NiTAPP-EDOT).

3.4 Electrochromic Studies

The electrochromic performance of the polymer thin films was systematically evaluated in the visible (575 nm) and bNIR (1020 nm) regions. Poly(MTAPP) thin films did not show any electrochromic response. In contrast, all three poly(MTAPP-EDOT) thin films displayed distinct color changes, appreciable optical contrast, fast switching kinetics (<2 s), good cycling stability, and excellent optical memory. This suggests a secondary contribution from the central metal atom in addition to the dominant influence of EDOT in the copolymers (Figure 18). The incorporation of EDOT played a critical role in enhancing electronic conductivity and facilitating counterion diffusion within the polymer matrix, thereby enabling efficient redox-driven optical modulation. Notably, poly(ZnTAPP-EDOT), and poly(H_2TAPP-EDOT) thin films exhibited two distinct and reversible color states, whereas the poly(NiTAPP-EDOT) thin film displayed three well-defined color states (Image 2) during switching cycles. This multichromic behavior in poly(NiTAPP-EDOT) thin film is attributed to the additional redox activity and electronic contribution of the Ni, which modulates the electronic structure of the porphyrin macrocycle during doping and dedoping processes.

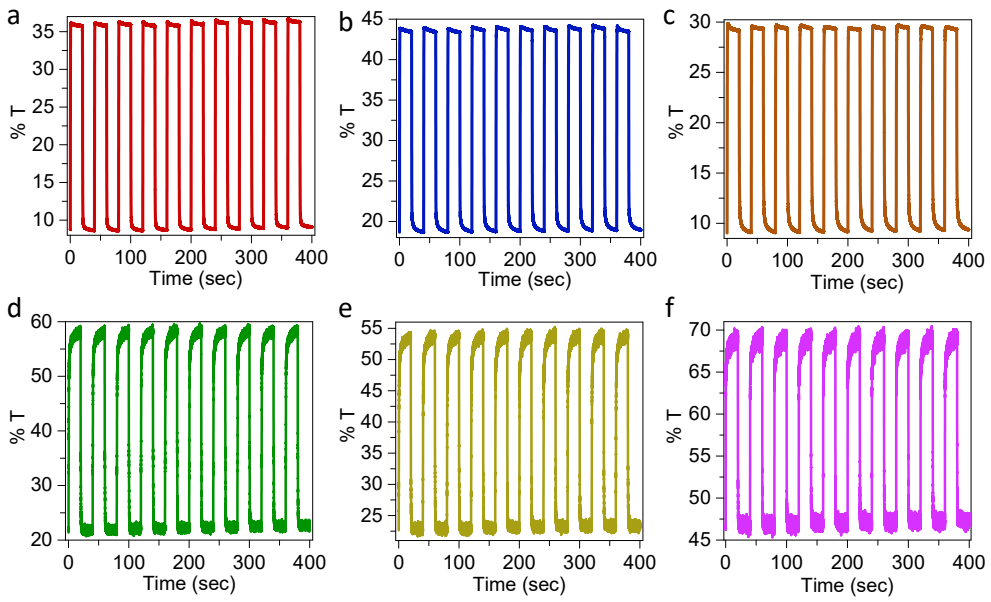

Figure 18. (a-c) Transmittance changes monitored at 575 nm for poly(NiTAPP-EDOT), poly(ZnTAPP-EDOT), and poly(H_2TAPP-EDOT), (d-f) corresponding responses at 1020 nm.

Among the series (Table 6), poly(ZnTAPP-EDOT) exhibited the shortest oxidation time at 575 nm (t_{ox} = 0.36 s), indicating rapid charge transport within the polymer film. In the NIR region, however, poly(H_2TAPP-EDOT) showed a comparatively faster oxidation time relative to the metalated analogues. Reduction times were consistently longer across all polymers, which can be attributed to the slower kinetics of ion reinsertion during the reduction process. In terms of optical contrast, poly(NiTAPP-EDOT) achieved ΔT% values of 27.3% at 575 nm and 37.5% at 1020 nm. A progressive decrease in ΔT% from Ni to Zn to free-base systems indicates that metal coordination enhances π-conjugation and charge delocalization, thereby improving optical modulation. Regarding long-term electrochromic stability, poly(ZnTAPP-EDOT) demonstrated the highest retention at 575 nm (97.1%), followed by poly(NiTAPP-EDOT) (93.6%) and poly(H_2TAPP-EDOT) (91.6%), with a similar trend observed at 1020 nm after 100 cycles. Furthermore, minimal variation in transmittance at 575 nm and 1020 nm under alternating potential conditions (2 s pulses with a 200 s open-circuit interval) indicates excellent optical memory for all polymer films (Figure 19). Overall, these results demonstrate that the central metal atom plays a decisive role in governing the electrochromic response, color modulation, and switching behavior of porphyrin-based copolymers. A detailed discussion of the electrochromic properties and comparative analysis of these systems is presented in papers I & II. CIE L*a*b* color coordinates and CIE chromaticity coordinates (x, y, z) of the thin films are presented in Table 7.

Table 6. Electrochromic properties of polymer thin films.

Polymer	System	Wavelength (nm)	t_{ox} (s)	t_{red} (s)	ΔT (%)	EC stability after 100 cycles
Poly(NiTAPP-EDOT)	0.1M $TBAPF_6$ / ACN	575	0.43	0.79	27.3	93.6
		1020	0.63	1.85	37.5	86.7
Poly(ZnTAPP-EDOT)		575	0.36	0.67	25.2	97.1
		1020	0.74	1.88	31.1	92.2
Poly(H_2TAPP-EDOT)		575	0.51	1.38	20.2	91.6
		1020	0.45	1.42	23.9	83.9
Poly(NiTAPP-EDOT)	Aqueous 4m $ZnCl_2$	560	0.31	1.59	17.5	95.9

Table 7. CIE L*a*b* color coordinates and CIE chromaticity coordinates (x, y, z) reflecting the electrochromic color evolution of each polymer.

Polymer	Potential (V)	L	a	b	x	y	z	ΔE
Poly(NiTAPP-EDOT)[a]	-0.5	40.91	-3.14	-1.53	0.33	0.35	0.30	42.7
	0.7	72.36	-6.29	27.14	0.38	0.42	0.19	
Poly(ZnTAPP-EDOT)[a]	-0.5	54.70	-1.84	-6.67	0.33	0.34	0.33	25.7
	0.5	78.84	-5.94	14.52	0.36	0.39	0.24	
Poly(H_2TAPP-EDOT)[a]	-0.5	50.00	0.46	26.9	0.41	0.42	0.15	14.0
	0.5	67.20	-6.29	39.23	0.41	0.44	0.4	
Poly(NiTAPP-EDOT)[b]	-0.4	58.97	1.44	17.22	0.39	0.39	0.21	14.6
	0.5	70.99	-3.82	23.64	0.38	0.41	0.20	

[a] in 0.1 M $TBAPF_6$/ACN and [b] in aqueous 4 m $ZnCl_2$.

To evaluate performance in a more environmentally benign electrolyte, poly(NiTAPP-EDOT) was investigated in aqueous 4 m $ZnCl_2$ electrolyte 560 nm (Figure 20a,c). Poly(NiTAPP-EDOT) exhibited the fastest oxidation switching time in the study (t_{ox} = 0.31 s), outperforming its performance in the organic system. The reduction time was comparatively longer, indicating asymmetric switching kinetics. The optical contrast in the aqueous system (ΔT = 17.5%) was lower than observed in the organic electrolyte. However, poly(NiTAPP-EDOT) demonstrated excellent electrochromic stability, retaining 95.9% of its initial performance after 100 cycles, and demonstrated good optical memory.

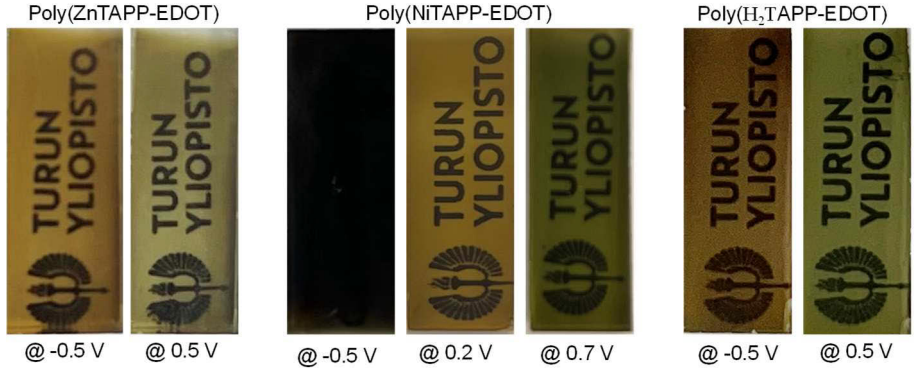

Image 2. From left to right, colors of the thin films at different potentials for poly(ZnTAPP-EDOT), poly(NiTAPP-EDOT), and poly(H_2TAP-EDOT) in 0.1 M $TBAPF_6$/ACN on the FTO electrode surface.

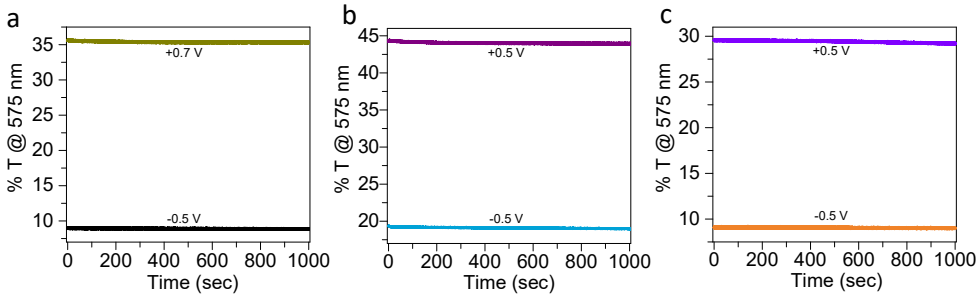

Figure 19. Chromic memory of (a) poly(NiTAPP-EDOT), (b) poly(ZnTAPP-EDOT), (c) poly(H_2TAPP-EDOT) thin film in 0.1 M $TBAPF_6$/ACN on the FTO electrode surface.

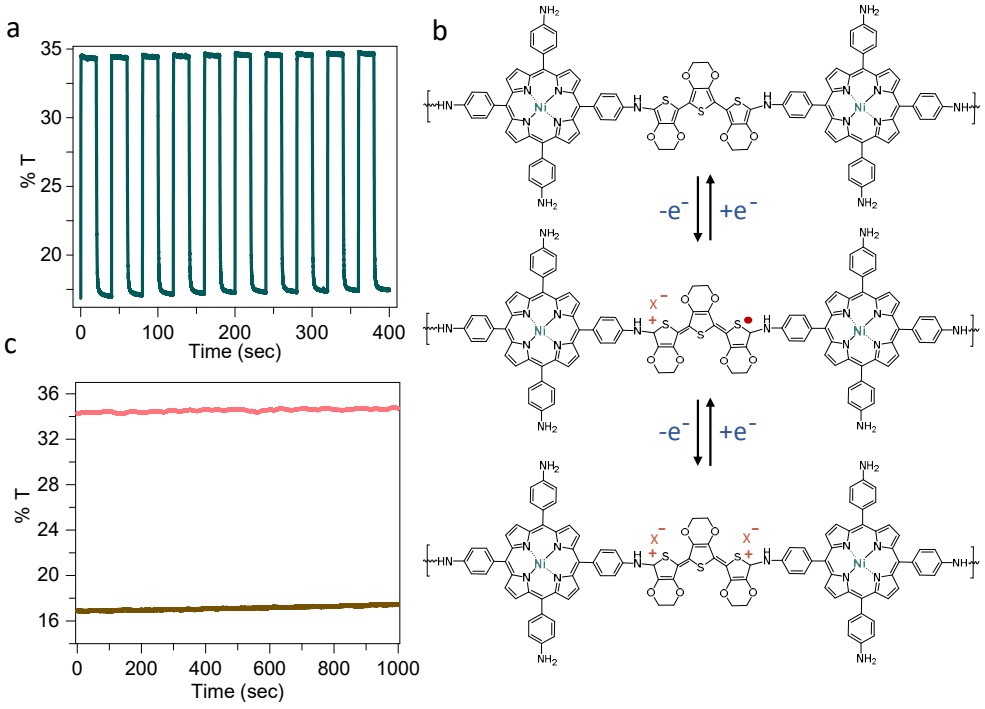

Figure 20. (a) Electrochromic switching behavior and (c) chromic memory of poly(NiTAPP-EDOT) thin film in aqueous 4 m $ZnCl_2$ electrolyte. (b) Schematic representation of polaron and bipolarons formation in the poly(NiTAPP-EDOT) thin film.

3.5 Supercapacitors

Electrochemical characterization of the poly(NiTAPP-EDOT) thin film was performed in 4 m $ZnCl_2$ electrolyte in a three-electrode configuration, with a Pt wire and a quasi Ag/AgCl wire serving as the counter and reference electrodes, respectively (Figure 21). The 4 m $ZnCl_2$ solution has the highest ionic conductivity compared to other $ZnCl_2$ concentrations[143]. Cyclic voltammetry (CV, scan rate (ν) = 5-200 mV s^{-1}), galvanostatic charge-discharge (GCD, current density (J) = 0.03-2 mA cm^{-2}), and electrochemical impedance spectroscopy (EIS, frequency = 0.3 MHz - 2 mHz; 10 mV constant potential) techniques were used to evaluate capacitance, long-term cycling stability, equivalent series resistance (ESR), and charge transfer resistance (R_{CT}) of the material.

The quasi-rectangular shape of the CV curves indicates that charge storage occurs predominantly via electric double-layer (EDL) formation at the electrode-electrolyte interface. The rectangular shape was maintained even at higher scan rates up to 200 mV s^{-1}, suggesting efficient charge percolation-depercolation within the active electrode. Additionally, the large enclosed area of the CV curves reflects a high charge-storage capacity of the poly(NiTAPP-EDOT) thin film. The triangular nature

of the GCD profiles further supports the CV analysis of the EDL-dominated charge storage mechanism. At lower current densities, the potential drops (V = IR, where I is current and R is resistance) are minimal, indicating high charge mobility at the electrode interface, which is essential for achieving high capacitance and power density in the material. The GCD profiles also show relatively short charging times and longer discharging times. The capacitance of the poly(NiTAPP-EDOT) thin film was calculated from the GCD curves using the formula given in the experimental section and plotted against current density.

The specific capacitance of the poly(NiTAPP-EDOT) thin film, calculated from the GCD curves, reaches 8.7 mF cm^{-2} at a current density of 0.03 mA cm^{-2}. The capacitance retains approximately 50% of its initial value at higher current densities, indicating good rate capability and low internal resistance. From EIS analysis, the Nyquist plot appears nearly parallel to the imaginary axis in the lower-frequency region, with a very small semicircle in the higher-frequency region (zoomed-in section), indicating nearly ideal capacitive behavior, low R_{CT}, and efficient electrolyte diffusion. The ESR and R_{CT} values are approximately 66.5 Ω and 4.5 Ω, respectively. Furthermore, the time constant ($\tau_o = 1/f_o$; where f_o is the frequency at a phase angle of -45°) of the poly(NiTAPP-EDOT) thin film, calculated from the Bode phase plot, is approximately 2.65 s.

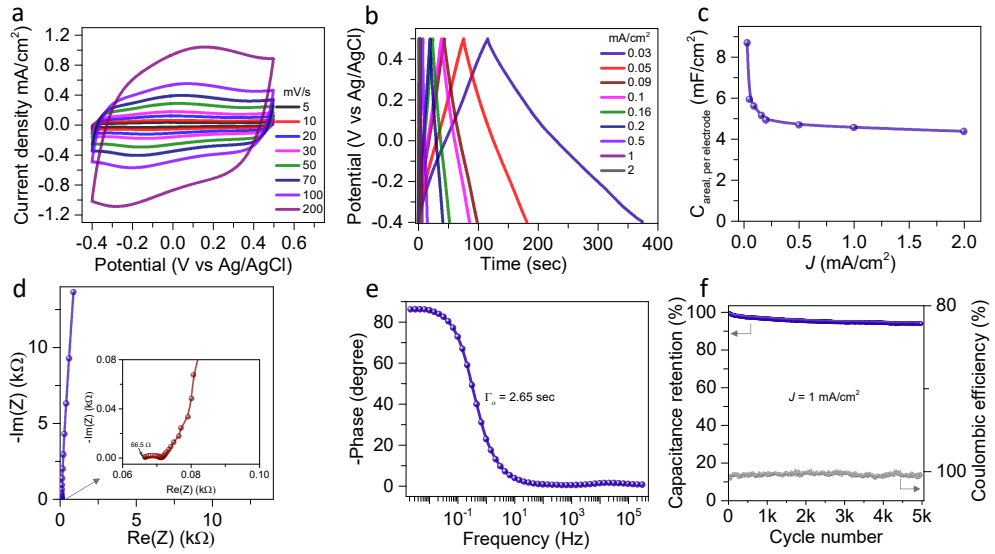

Figure 21. (a) CV, (b) GCD, (c) Capacitance vs current density, (d) Nyquist (inset: zoomed-in at high frequency region), (e) Phase, and (f) Long-term cycling stability plots of poly(NiTAPP-EDOT) thin film in aqueous 4 m $ZnCl_2$ electrolyte.

The long-term cycling stability of the poly(NiTAPP-EDOT) thin film electrode was evaluated by performing 5000 continuous GCD cycles at a current density of 1 mA cm^{-2}. Notably, the poly(NiTAPP-EDOT) thin film retained >90% of its capacitance with approximately 100% Coulombic efficiency, suggesting excellent robustness and facile charge percolation throughout the GCD cycles.

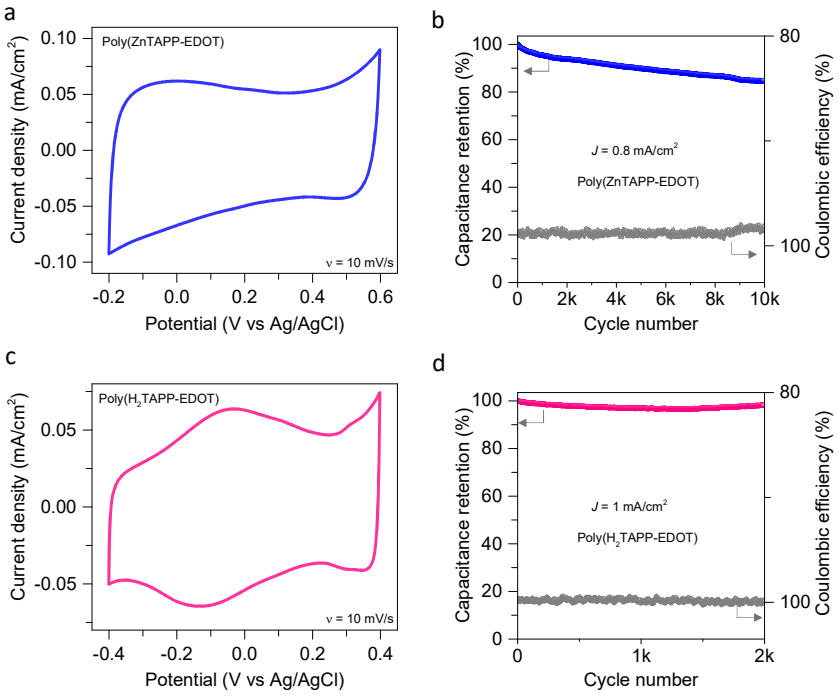

Figure 22. CV and long-term cycling stability plots of (a-b) poly(ZnTAPP-EDOT) and (c-d) poly(H_2TAPP-EDOT) thin film in aqueous 4 m $ZnCl_2$ electrolyte.

We also tested the electrochemical performance of poly(ZnTAPP-EDOT) and poly(H_2TAPP-EDOT) copolymer thin films in a 4 m $ZnCl_2$ electrolyte (Figure 22). Here, preliminary data are presented to demonstrate the potential of these copolymer thin films for supercapacitor applications. The poly(ZnTAPP-EDOT) and poly(H_2TAPP-EDOT) copolymer thin films showed EDLC characteristics and long-term cycling stability of about 85% (after 10,000 GCD cycles) and 98% (after 2,000 GCD cycles), respectively, indicating that these materials are excellent candidates for supercapacitor electrodes.

3.6 Density Functional Theory Study

Time-dependent density functional theory (TD-DFT) calculations were performed to gain deeper insight into the electronic structure and optical properties of the porphyrin-EDOT copolymers and to support the experimental observations. Model oligomers containing varying numbers of EDOT linkages between porphyrin units were investigated to evaluate the effect of conjugation length and structural arrangement. Additionally, MTAPP and EDOT oligomers were calculated as references, and their individual electronic contributions were assessed (papers I & II). The simulations revealed a systematic redshift in the absorption bands with increasing EDOT content, primarily arising from $\pi \rightarrow \pi^*$ transitions localized on the porphyrin macrocycles. This redshift, accompanied by enhanced oscillator strengths, is attributed to extended π-delocalization facilitated by additional EDOT linkages. Frontier molecular orbital analysis showed that the HOMO-LUMO transitions responsible for these absorption features are mainly distributed along the conjugated backbone, with the LUMO in MTAPP-$(EDOT)_3$-MTAPP significantly delocalized across the entire molecular framework (papers I & II). The TD-DFT spectra were in agreement with the experimental UV-Vis studies, supporting the proposed copolymer structure and a mechanistic pathway in which multiple EDOT units preferentially bridge adjacent MTAPP moieties, thereby promoting efficient charge carrier delocalization.

In a separate study, DFT calculations were performed to investigate the electropolymerization mechanism, the influence of the central metal atom (Zn^{2+} vs Ni^{2+}), and the effect of keto functionalization on polymer formation. In ZnOEPK, the HOMO is predominantly localized around the central Zn atom, as well as adjacent N and C atoms, while the LUMO is more delocalized near the keto group (Figure 24a,c). In contrast, NiOEPK exhibits a more delocalized HOMO distributed across the porphyrin macrocycle (excluding the nitrogen atoms), while the LUMO is concentrated around the central metal atom (Figure 24b,d). These differences in electronic structure dictate the preferred site for nucleophilic attack by the first 4,4′-bpy molecule. Specifically, the meso position nearest to the keto group (position 20) is favored in ZnOEPK, whereas the meso position farthest from the keto group (position 10) is preferred in NiOEPK. Furthermore, DFT calculations predict that the second 4,4′-bpy unit preferentially attaches at the meso position opposite to the first substitution site in both systems. In both cases, the bipyridine units adopt parallel orientations perpendicular to the porphyrin plane, thereby promoting directional and linear polymer growth (paper III).

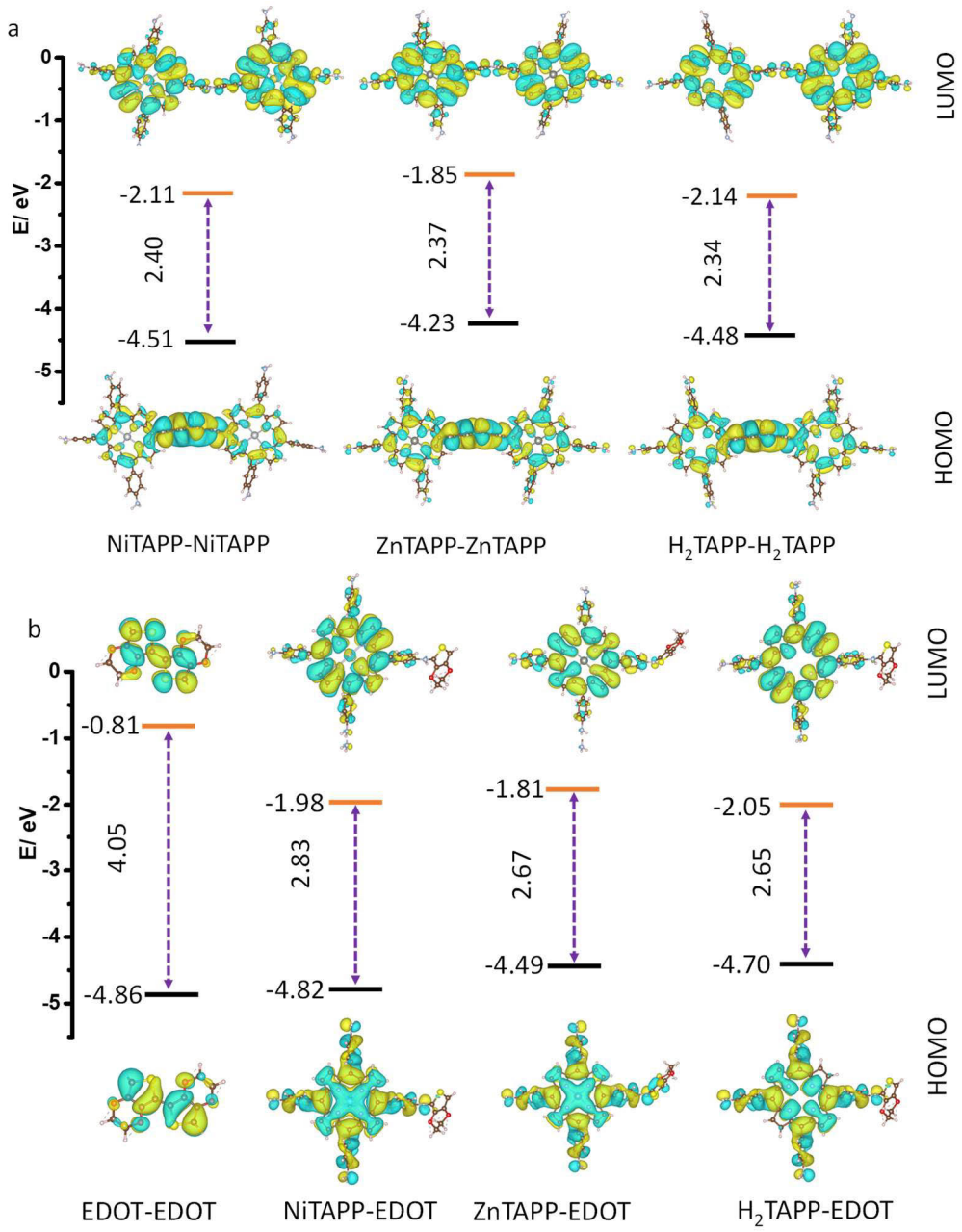

Figure 23. Frontier molecular orbital isosurface plots of the HOMO and LUMO (highest occupied and lowest unoccupied molecular orbitals) calculated for the optimized dimer structures, illustrating the spatial distribution and extent of electron density delocalization across the conjugated backbone.

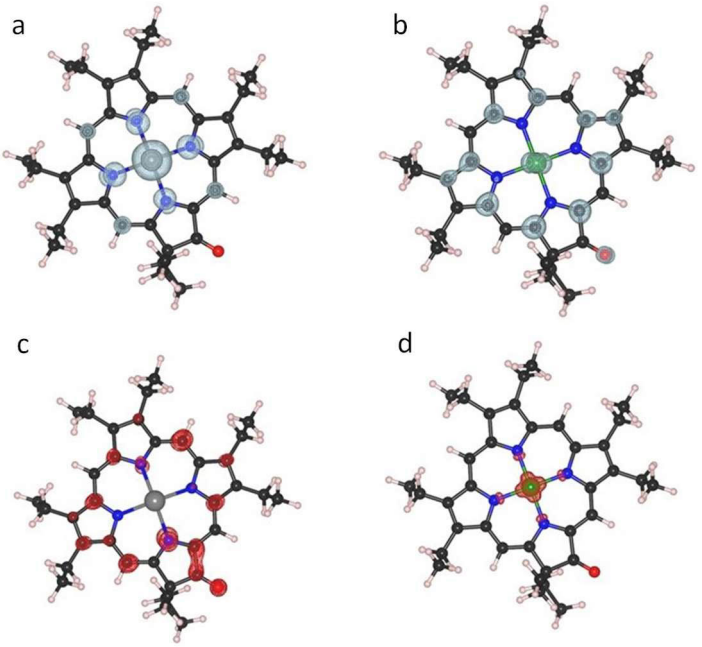

Figure 24. Frontier molecular orbital isosurface plots of the (a, b) HOMO and (c, d) LUMO (highest occupied and lowest unoccupied molecular orbitals) calculated for the optimized structures for ZnOEPK and NiOEPK, respectively.

4 Conclusion

Porphyrins represent a versatile class of π-conjugated macrocycles with tunable electronic, optical, and redox properties, making them highly attractive building blocks for advanced functional materials. Their structural flexibility, ability to coordinate different metal centers, and rich photophysical behavior enable precise control over charge transport and light-matter interactions. Electropolymerization of porphyrins provides a direct route to electroactive thin films, in which the intrinsic properties of the macrocycle are preserved and amplified within a conjugated polymer framework. In this thesis, porphyrin-based homopolymer and copolymer thin films were successfully synthesized on FTO glass substrates via an efficient electrocopolymerization approach and were tested for ECSC performance in both organic and aqueous electrolytes.

Meso-aminophenyl-substituted porphyrins (MTAPP; M = Zn^{2+}, Ni^{2+}, H_2) were electropolymerized through oxidative coupling of the aminophenyl substituents to form homopolymer thin films via phenazine and dihydrophenazine linkages. These monomers were also electrocopolymerized with EDOT to generate conjugated copolymer networks. The progressive increase in current during successive cyclic voltammetry scans confirmed continuous and reproducible film growth on conductive substrates. The resulting films exhibited well-defined morphologies while preserving the structural integrity of the porphyrin core.

Comprehensive characterization by UV-Vis, Raman, FTIR, XPS, AFM, and SEM confirmed the structural and electronic properties of the films. UV-Vis spectra showed characteristic red shifts and broadening of the Soret and Q-band upon polymerization, consistent with extended π-conjugation and enhanced electronic delocalization. In situ UV-Vis measurements revealed reversible bleaching of π-π* transition and the emergence of polaron and bipolaron absorption bands in the bNIR, confirming an efficient and reversible doping-dedoping process. In situ Raman spectroscopy provided complementary molecular-level insight, with systematic shifts in the C_α=C_β stretching modes indicating backbone reorganization during electrochemical doping. The broader distribution of conjugation lengths observed in poly(MTAPP-EDOT) relative to regioregular PEDOT reflects the structural heterogeneity introduced by porphyrin incorporation.

The electrochromic performance of the porphyrin-EDOT copolymers demonstrated rapid switching (< 2 s), appreciable optical contrast in both visible and NIR regions, good coloration efficiency, and excellent optical memory. Copolymerization with EDOT significantly enhanced electrochromic response compared to porphyrin homopolymers, highlighting the critical role of EDOT in enabling efficient charge-carrier-driven optical modulation. The central metal ion further influenced the accessible color states: poly(ZnTAPP-EDOT) and poly(H_2TAPP-EDOT) exhibited two reversible color states, whereas poly(NiTAPP-EDOT) displayed three distinct states. This behavior is attributed to the additional redox activity of the Ni^{2+} center and its influence on the electronic structure of the porphyrin macrocycle, demonstrating that metal coordination provides an effective strategy for tuning electrochromic behavior.

The copolymer thin films were tested for electrochromic supercapacitor applications in 4 m $ZnCl_2$ aqueous electrolyte. Poly(NiTAPP-EDOT) exhibits EDLC characteristics, delivering a specific capacitance of 8.7 mF cm^{-2} and retaining over 90% capacitance after 5000 GCD cycles with nearly 100% Coulombic efficiency. Similarly, poly(ZnTAPP-EDOT) and poly(H_2TAPP-EDOT) also displayed EDLC characteristics and retain 85% and 98% of their capacitance after 10,000 and 2,000 GCD cycles, respectively. To the best of our knowledge, this represents the first demonstration of electropolymerized porphyrin copolymers functioning as electrochromic supercapacitors in a concentrated aqueous electrolyte, highlighting their potential for sustainable multifunctional energy storage applications.

In addition, keto-functionalized octaethylporphyrins (MOEPK; M = Zn^{2+}, Ni^{2+}) were electropolymerized using 4,4′-bipyridine as a bifunctional bridging nucleophile, enabling direct polymer formation without the need for pre-functionalized monomers.

Theoretical investigations provided further insights into the optical properties and polymer growth mechanisms. TD-DFT calculations revealed systematic red shifts in absorption as the number of EDOT units in the linkage increased, confirming that extended π-delocalization along the conjugated backbone governs the optical behavior of the copolymers. DFT studies of keto-functionalized porphyrins clarified the role of the central metal in regioselective nucleophilic attack during electropolymerization. ZnOEPK favored substitution at the meso position adjacent to the keto group (position 20), whereas NiOEPK preferentially reacted at the opposite site (position 10). In both systems, sequential 4,4′-bipyridine attachment at opposing meso positions promoted directional and linear polymer growth.

Overall, this work establishes a comprehensive structure-property framework for porphyrin-based electroactive polymers, demonstrating how molecular design, metal coordination, polymerization strategy, and electrolyte environment collectively govern optical, electronic, and electrochemical performance. These findings provide

a strong foundation for the development of tunable multicolor electrochromic devices and integrated electrochromic energy-storage systems based on porphyrin electropolymer platforms.

5 Future Scope

The electrocopolymerization strategy established in this work opens multiple avenues for future research, particularly in extending this approach to a broader range of porphyrin-monomer copolymer systems for smart material applications. Systematic exploration of different monomer combinations is expected to enable the development of copolymers with enhanced and tunable properties, especially for electrochromic energy-storage applications. As an initial demonstration, a preliminary study on poly(H_2TAPP-azulene) copolymers has already shown promising electrochemical performance.

The systematic variation of the central metal atom in metalloporphyrins, as demonstrated in this work, provides a viable strategy for designing multicolor electrochromic supercapacitor systems. The strong electrochromic supercapacitor performance of porphyrin-EDOT copolymer thin films in concentrated aqueous electrolytes represents an important step toward sustainable electrochemical technologies. Furthermore, the implementation of water-in-salt electrolytes (WiSEs) offers a promising route to extend the electrochemical stability window beyond 2 V, which could significantly enhance both the operating voltage and energy density of porphyrin-based electrochromic supercapacitors.

Beyond electrochromism and energy storage, the unique physicochemical properties of porphyrin-based thin films make them attractive for a wide range of advanced applications, including electrochemical sensing, solar energy conversion, flexible electronics, and wearable electrochemical devices.

Acknowledgements

I would like to begin by thanking the University of Turku for providing an excellent learning environment and valuable opportunities throughout my PhD journey. I am also grateful to the Department of Chemistry for its inspiring research atmosphere and to the Doctoral Programme in Exact Sciences (EXACTUS) for the opportunity to pursue my doctoral degree. I am grateful for financial support from Magnus Ehrnooth Foundation, Fortum and Neste Foundation, Real Estate Foundation, Business Finland, Department of Chemistry, and the University of Turku.

I would like to extend my gratitude to Professor Aline Rougier and Professor Laurent Ruhlmann for accepting to review my thesis and for the time and effort devoted to its evaluation. My special thanks to Professor Eunkyoung Kim for accepting to serve as the opponent for my thesis defense. Your presence at this important milestone means a great deal to me.

I would like to express my sincere gratitude to my supervisor and research director, Professor Carita Kvarnström, for her support, guidance, and encouragement throughout my doctoral studies. Her expertise and insightful discussions were invaluable to this work. Beyond research, I truly appreciate the warmth shared by Carita and her sister Stina during visits to their summer cottage and Christmas lunch, which made this journey all the more memorable.

I am also deeply thankful to my co-supervisors, Dr. Pia Damlin and Dr. Mikko Salomäki, for their support, feedback, and guidance throughout this project. A special thanks to Dr. Pia Damlin for always being there for me and for introducing me to the fascinating world of in situ spectroelectrochemistry, a technique that became an important and enjoyable part of my research journey. I would also like to especially thank Dr. Mikko Salomäki for his invaluable help with AFM and XPS.I would like to thank my collaborators, Dr. Shweta Mehta, Dr. Kavita Joshi, and Dr. Subrahmanyam Sappati, for their valuable contributions to the theoretical studies. I am also grateful to Sari Granroth for teaching me XPS, to Ermei Mäkilä for providing SEM images, and to Dr. Niko Meltola for providing the porphyrins used in this work. I would also like to sincerely thank Emeritus Professor Jukka Lukkari. As an early reviewer of both my papers and thesis, your feedback, insights, and

thoughtful perspective have always been invaluable and have greatly contributed to my growth as a researcher.

I express my sincere gratitude to Dr. Plawan Kumar Jha, aka Plawan bhai. Words can hardly express how much I have learned from you. Thank you for introducing me to the world of supercapacitors. This greatly enriched this work and broadened my scientific perspective. More importantly, you changed the way I looked at research, teaching me to question, analyze, and think beyond the written words of a research article, and nurturing my curiosity for science. I deeply value the friendship we built along the way.

My special thanks to Kari, Mauri, and Kirsi. Kari, the department has not felt the same since your retirement. I will always miss your readiness to help and your willingness to go beyond your duties. Mauri, thank you for the beautifully crafted cells and reactors; your attention to detail truly made research easier. Kirsi, thank you for everything throughout this journey. Without your help, I might still be trying to navigate all those special chemicals.

No PhD journey survives without good labmates. This journey was made lighter by good science, caffeine, sarcasm, and wonderful people.

To Dr. Rahul, thank you for your friendship, for introducing me to electrochemistry, and for the many discussions that made both science and life easier to navigate. Beyond the lab, thank you for all the road trips, camping, trekking, good food, and cycling adventures. To Dr. Lokesh Kesavan, thank you for the calm presence and conversations that made ordinary days better. To Dr. Milla Vikberg, thank you for the scientific discussions, collaboration, and for sharing the cabin. To Dr. Adefunke, sharing the same birth date and nearly the same research topic made our friendship uniquely memorable. To Ashwini Jadhav, sharing the highs, lows, deadlines, small victories, travel diaries, and crazy outings made this PhD far more meaningful. To Majid, thank you for bringing humor to difficult days and of course, “Go Pokémon Go! To Vinh, simply the best, thank you for the long conversations that somehow covered everything around the world. To Joona, thank you for your positivity and great collaboration. To Pulmu, thank you for your kindness. To Roni, thank you for the time spent working together on water purification. To Ali Tuna, thank you for helping me better understand porphyrins from the synthesis perspective. To Dr. Rajeswari, thank you for the lunch sessions, discussions, and collaborations. To Atte, thank you for helping me use the densitometer and viscometer. To master's thesis students, Felix and Adiba, thank you for making supervision a shared learning experience.

My heartfelt thanks also go to our Heads of Department, first Professor Pasi Virta and now Professor Mika Lastusaari, for your support throughout my PhD journey. I am especially grateful for the opportunity to participate in the Global Young

Scientists Summit in Singapore, an experience that remains one of the most memorable highlights of my PhD journey.

Dr. Ari Lehtonen and Dr. Harri Harma, thank you for the wonderful conversations and positivity that made everyday lab life brighter. To Dr. Anssi Peuronen, thank you for your kindness and help, especially with XRD. To Narhari, a businessman disguised as a PhD student, thank you for the laughs, research collaboration, and memorable company. To Ville, thank you for your nice talk and help with the freeze dryer. To the IMC family, Isabella, Emilia, Minnea, Sami, Hannah, Cecilia, Ian, Leo, Pasi, Amritha, Bettina, Joshua, Pinja, and Natalia, thank you for the conversations and memorable company. To the SMAT research group, Mahsa, Anamika, Mohammad, Pelin, Ceylin, and Maryam, thank you for the coffee breaks, conversations, and laughter. To the chemistryUTU Instagram group, Maarit, Päivi, and the one and only Sami, thank you for the creativity and teamwork behind all the posts and content.

Research may have brought us together in Finland, but friendship made the journey worthwhile. To Santosh, Preeti, and Veda, thank you for making me feel at home while being miles away from it. Your warmth and companionship meant more than words can express. To Senthil, thank you for your friendship, for keeping me accountable even on the days I wanted to skip workouts, and for the memorable road trips. To Kedar and Renuka, thank you for making moments away from home feel warm and familiar. Kedar, for the conversations and life lessons, and Renuka, for always accommodating my dietary quirks. And Aaru made every gathering even more special. To Kriti, thank you for your friendship and for the thoughtful gestures that always made special occasions brighter. Thank you for introducing me to new cuisines and for the wonderful cakes that made celebrations extra special. The best is always in the details, and you are truly that person. To Bishweshwar, Debangana, and Anu, thank you for the meals, cycling trips, and wonderful moments together. Bishu, a special thank you for introducing me to trading and badminton, which added even more fun to this journey.

To the group where fun always came with its own warning label, from organizing events, dancing, and shared chaos, thank you for all the get-togethers, laughter, and for making this journey more vibrant. Rahul, thank you for all those long runs, trekking adventures, cycling, festivities, and the many good memories and medals along the way. Jismi, thank you for your organizational skills and for surviving committee chaos together. Sibi, thank you for always being part of the madness. To Omkar (Sirji), thank you for all the wonderful times, thoughtful conversations, and for always being such great company. Dr. Shruti, thank you for sharing the experience from the 3MT thesis competition to the Millennium Pitching Contest. Afshan, thank you for the wonderful group pictures, long conversations, and dance lessons. Dr. Madhukar and Uma, despite meeting late, it was amazing how similar

our paths felt. Mayank, thank you for your thoughtful questions and perspective. Joakim, what started through Ashwini turned into a valued friendship. And to the newest addition to the group, Elango, you brought the biggest smiles.

To Gopala, writing our theses brought an unexpected friendship and mutual support. Thank you for being there when I needed it most, often without me even having to ask. To all the wonderful people I met during this journey in Finland Prasanna, Amruta, Ira, Ameya, Vipin, Ankita, Binu, Luv, Priyanka, Arjun, Kushagra, Debango, Alan, Shishir, Nitin, Avlokita, Partibhan, Kalai, Amresh, Shivkumar, Kamlesh, Magilan, Janita, Robert, Aravind, Pinja, Mira, Eelis, Bahar, Elias, Mikael, Gunilla, Hanna, Elin, Anti, Vincent, Anna, and Patrik, thank you for making life in Finland warmer and more memorable.

And finally, to the people back home in India who stood by me despite the distance, time zones, and missed moments, your love and support always reached me, no matter how far Finland felt. To my parents, Pranita (Mom) and Prakash (Dad) Kochrekar, words will never be enough to thank you for all the sacrifices, love, and unwavering support. Through every success, setback, and moment of doubt, you stood beside me with constant faith. To Sushant (Appy) and Roshani, thank you for being there when I could not be. Your support meant more than words can express.

To my extended family, Rajan (Mama), Arun (Mama), Ashok (Mama), Shobha (Mavsi), Lata (Mami), Bharti (Mami), Sangeeta (Mami), and Deepa (Kaki), thank you for your love, support and for always being part of my life despite the distance. To my gang, my people through everything, Ravi, Sai, Sharad, Supriya, Nisha, Rajita, Rohit, Roshan, Rohan, Megha, Bhagya, Darshan, Pranay, Prasanna, and Pratibha, I feel incredibly blessed to have shared this journey of life with all of you. Along the way, our circle only grew bigger and stronger with the wonderful additions of Ashwini, Pranali, Shweta, Mayur, and Shyam. And then came the next generation, Vipul, Samartha, Riya, Ayush, Arush, Dhimit, Trinaini, and Laksha, bringing even more joy and reminders that happiness is often found in the smallest moments.

To the one and only Ekta Kotharkar, my partner in crime, my better (more than) half, and my forever place to call home. Life, and certainly this journey, would not have been as easy or as beautiful without you by my side. Thank you for bringing that little extra spice into my life and for making even the ordinary moments feel truly special. Thank you for being my strength, especially on the days when the road ahead felt uncertain, for pushing me when I doubted myself, for grounding this overthinking mind, and for somehow teaching me to think a little straighter and simpler. Your patience, love, belief in me, and unwavering support carried me through more moments than words can ever express. Through every high and low, you remained my calm, my comfort, and my biggest cheerleader. This journey would simply not have been the same without you. And thank you for bringing into my life a wonderful family, Savita (Mummy), Uday (Pappa), and Sunny Kotharkar. Thank

you for welcoming me with open hearts; your kindness, support, and affection mean far more than words can express. To the ever-energetic bacha party, Shubham, Sakshi, Sejal, Dipti, Payal, Palak, Prachi, Ansh, and Sony, thank you for the laughter, madness, joy, and countless happy moments.

To Vilas Gadre, Sir, your knowledge and ability to think beyond boundaries have always inspired me. I would not be here writing this thesis without your support during one of the most difficult phases of my life. I owe an important part of this journey to your encouragement and life lessons. Heartfelt thanks also to Vaibhav Dada, Kshiti Tai, and Sanika. Thank you for always being there for me.

To my childhood friends, Tulsidas, David, Amit, Jairam, and Shringar, thank you for the unforgettable childhood memories and for a bond that has only grown stronger with time. To my backseat boys, Rohit, Sujay, Vishal, Abhijit, Swapnil, Aniket, and Sagar, thank you for the chaos, laughter, and memories that still bring a smile. To my bachelor's, master's, and Pune friends, Krishna, Viraj, Ashwin, Newton, Dr. Johnross, Rakesh, Keshav, Monali, Jagruti, Prajvi, Dr. Pooja, Deseree, Crezel, Priyanka, Sneha, Kiran, Sitaram, Mandar, Pravin, Bhavesh, Nikhil, Vinod, Sudhir, Deepti, Manjunath, Rupesh, Shailesh, Gautam, Dr. Yadnesh, Dr. Prakash, Dr. Vandana, Dr. Satish, Dr. Sulakshana, Dr. Sonia, Dr. Sudhakar, Dr. Anuja, Dr. Shivaji, Dr. Gajanan, and Pallavi, thank you for the friendship, shared experiences, and countless memories that made those years truly memorable. From classrooms to celebrations, shared struggles to laughter, those moments will always remain special. The same gratitude extends to my study buddies, Navnath, Dr. Sandeep, Sachin, Ganesh, Dr. Laxman, Dhalpe, Kapil, and Dr. Shankar, for the long hours of studying, preparing for exams, and learning from one another. A special thanks also to my dear friend and flatmate, Dr. Chetan Chavan, for the friendship, companionship, warmth, and wonderful memories that made those years even more meaningful. I am equally thankful to my labmates, Mahesh, Dr. Musibau Azeez, Dr. Sachin Pansare, Dr. Mrunal, Dr. Hidouri Slah, Dr. Bhaskar, Dr. Pinky, Dr. Hema, Dr. Deepak, Neha, Annaya, and Arvind. Each of you contributed to this journey through friendship, shared learning, support, and memories that I will always carry with a smile. To Professor Shibal Banerjee, thank you for your mentorship and guidance, which played an important role during my time in Pune.

And finally, to the loved ones and family members I lost along the way, I am grateful for every memory and lesson. Though you are no longer physically here, your presence lives on in my heart and in the person I continue to become.

Through every rise and fall, faith remained constant. Ganapati Bappa Morya!

22 May 2026, Turku
Sachin Kochrekar

List of References

1 F. Xia and L. Jiang, *Adv. Mater.*, 2008, **20**, 2842–2858.
2 Y. Liu, J. Tang, R. Wang, H. Lu, L. Li, Y. Kong, K. Qi and J. H. Xin, *J. Mater. Chem.*, 2007, **17**, 1071–1078.
3 H. Lee, B. P. Lee and P. B. Messersmith, *Nature*, 2007, **448**, 338–341.
4 P. V. Navya and S. Sampath, *Chem. Asian J.*, 2025, **20**, 202401724.
5 R. Hanlon, *Curr. Biol.*, 2007, **17**, R400–R404.
6 Y. Yin and J. A. Rogers, *Chem. Rev.*, 2022, **122**, 4885–4886.
7 K. K. Kushwah, S. Jindal, A. K. Vyas and P. Chatterjee, *Smart Materials and Applications*, Apple Academic Press, New York, 2025.
8 K. Kumar and Chikesh. Ranjan, *Smart Materials: Electro-Rheological Fluids, Piezoelectric Smart Materials, and Shape Memory Alloys*, Walter De Gruyter GmbH & Co KG, 2025.
9 S. Bahl, H. Nagar, I. Singh and S. Sehgal, *Mater. Today Proc.*, 2020, **28**, 1302–1306.
10 A. Mukherjee, Deepmala, P. Srivastava and J. K. Sandhu, *Mater. Today Proc.*, 2023, **81**, 350–359.
11 M. Vik and A. P. Periyasamy, *Chromic Materials*, Apple Academic Press, 2018.
12 N. M. Rowley and R. J. Mortimer, *Sci. Prog.*, 2002, **85**, 243–262.
13 P. Monk, R. Mortimer and D. Rosseinsky, *Electrochromism and Electrochromic Devices*, Cambridge University Press, 2007, pp. 25–32.
14 C. G. Granqvist, *Handbook of inorganic electrochromic materials*, Elsevier, 1995.
15 J. R. Platt, *J. Chem. Phys.*, 1961, **34**, 862–863.
16 S. K. Deb, *Appl. Opt.*, 1969, **8**, 192.
17 S. K. Deb, *Philos. Mag.*, 1973, **27**, 801–822.
18 H. Meng, *Organic Electronics for Electrochromic Materials and Devices*, Wiley, 2021.
19 D. R. Rosseinsky and R. J. Mortimer, *Advanced Materials*, 2001, **13**, 783–793.
20 R. J. Mortimer, *Chem. Soc. Rev.*, 1997, **26**, 147–156.
21 C. Gu, A. B. Jia, Y. M. Zhang and S. X. A. Zhang, *Chem. Rev.*, 2022, **122**, 14679–14721.
22 G. Cai, J. Wang and P. S. Lee, *Acc. Chem. Res.*, 2016, **49**, 1469–1476.
23 R. J. Mortimer, *Annu. Rev. Mater. Res.*, 2011, **41**, 241–268.
24 I. F. Chang, B. L. Gilbert and T. I. Sun, *J. Electrochem. Soc.*, 1975, **122**, 955–962.
25 D. Chen, M. H. Chua, Q. He, Q. Zhu, X. Wang, H. Meng, J. Xu and W. Huang, *Chem. Eng. J.*, 2025, **503**, 157820.
26 P. M. Beaujuge and J. R. Reynolds, *Chem. Rev.*, 2010, **110**, 268–320.
27 S. Kandpal, T. Ghosh, C. Rani, A. Chaudhary, J. Park, P. S. Lee and R. Kumar, *ACS Energy Lett.*, 2023, **8**, 1870–1886.
28 Y. Zhai, J. Li, S. Shen, Z. Zhu, S. Mao, X. Xiao, C. Zhu, J. Tang, X. Lu and J. Chen, *Adv. Funct. Mater.*, 2022, **32**, 2109848.
29 X. Li, K. Perera, J. He, A. Gumyusenge and J. Mei, *J. Mater. Chem. C Mater.*, 2019, **7**, 12761–12789.
30 R. J. Mortimer, A. L. Dyer and J. R. Reynolds, *Displays*, 2006, **27**, 2–18.
31 D. R. Rosseinsky and R. J. Mortimer, *Adv. Mater.*, 2001, **13**, 783–793.

32 P. J. Gellings, and H. J. Bouwmeester, *Handbook of solid state electrochemistry*. CRC Press, 2019.
33 P. M. S. Monk, R. J. Mortimer and D. R. Rosseinsky, *Electrochromism*, Wiley, 1995.
34 T. G. Yun, X. Chen and J. Y. Cheong, *Batter. Supercaps*, 2023, **6**, 202200454.
35 X. Yu, P. Guo, J. Chen, S. Li and H. Li, *Responsive Materials*, 2024, **2**, 20240013.
36 J. Kim, M. Rémond, D. Kim, H. Jang and E. Kim, *Adv. Mater. Technol.*, 5(6), 1900890.
37 X. Jiao, G. Li, Z. Yuan and C. Zhang, *ACS Appl. Energy Mater.*, 2021, **4**, 14155–14168.
38 Q. Guo, X. Zhao, Z. Li, B. Wang, D. Wang and G. Nie, *ACS Appl. Energy Mater.*, 2020, **3**, 2727–2736.
39 K. Wang, H. Wu, Y. Meng and Z. Wei, *Small*, 2014, **10**, 14–31.
40 T. Van Nguyen, Q. Van Le, S. Peng, Z. Dai, S. H. Ahn and S. Y. Kim, *Adv. Mater. Technol.,* 2023, 8(18), 2300474.
41 B. E. Conway, *Electrochemical Supercapacitors*, Springer US, Boston, MA, 1999.
42 Y. Shao, M. F. El-Kady, J. Sun, Y. Li, Q. Zhang, M. Zhu, H. Wang, B. Dunn and R. B. Kaner, *Chem. Rev.*, 2018, **118**, 9233–9280.
43 E. Frackowiak, *Phys. Chem. Chem. Phys.,* 2007, **9**, 1774.
44 E. E. Miller, Y. Hua and F. H. Tezel, *J. Energy Storage*, 2018, **20**, 30–40.
45 X. Jiao, J. Wang, Z. Yuan and C. Zhang, *Energy Storage Mater.*, 2023, **54**, 254–265.
46 C. Xiong, T. Wang, Z. Zhao and Y. Ni, *SmartMat*, 2023, 4(2), 1158.
47 L. Pradhan, T. K. Das and B. K. Jena, *Sustain. Energy Fuels*, 2025, **9**, 1917–1956.
48 D. S. Dalavi, R. S. Desai and P. S. Patil, *J. Mater. Chem. A Mater.*, 2022, **10**, 1179–1226.
49 D. Mohanadas and Y. Sulaiman, *J. Power Sources*, 2022, **523**, 231029.
50 X. Chen, Q. Liu, L. Cheng, S. Zhou, L. Chen, G. Liang, J. Wei and F. Mo, *Adv. Mater. Technol.*, 2024, **9**, 202301969.
51 Y. Shao, M. F. El-Kady, C. Lin, G. Zhu, K. L. Marsh, J. Y. Hwang, Q. Zhang, Y. Li, H. Wang and R. B. Kaner, *Adv. Mater.*, 2016, **28**, 6719–6726.
52 Z. Genene, Z. Xia, G. Yang, W. Mammo and E. Wang, *Adv. Mater. Technol.*, 2024, **9**, 2300167.
53 X. Guo and A. Facchetti, *Nat. Mater.*, 2020, **19**, 922–928.
54 J. Heinze, B. A. Frontana-Uribe and S. Ludwigs, *Chem. Rev.*, 2010, **110**, 4724–4771.
55 D. B. Tripathy and A. K. Jain, *Multifunctional materials: engineering and biological applications*, John Wiley & Sons, Inc.; Scrivener Publishing LLC, 2025.
56 K. Cao, D. E. Shen, A. M. Österholm, J. A. Kerszulis and J. R. Reynolds, *Macromolecules*, 2016, **49**, 8498–8507.
57 M. Heydari Gharahcheshmeh and K. Chowdhury, *Energy Adv.,* 2024, **3**, 2668–2703.
58 C. Friebe, M. D. Hager, A. Winter and U. S. Schubert, *Adv. Mater.*, 2012, **24**, 332–345.
59 T. Nezakati, A. Seifalian, A. Tan and A. M. Seifalian, *Chem. Rev.*, 2018, **118**, 6766–6843.
60 N. K and C. S. Rout, *RSC Adv.*, 2021, **11**, 5659–5697.
61 L. Groenendaal, G. Zotti, P. H. Aubert, S. M. Waybright and J. R. Reynolds, *Adv. Mater.,* 2003, 15(11), 855-879.
62 L. Cao, W. Zhang, B. Lu, C. Du, J. Zhang, W. Zhou, L. Zhao, X. Cheng, Y. Zhang, G. Zhang, J. Xu and L. Zhang, *J. Power Sources*, 2025, **657**, 238186.
63 C. L. Gaupp, D. M. Welsh, R. D. Rauh and J. R. Reynolds, *Chem. Mater.*, 2002, **14**, 3964–3970.
64 F. Jonas and L. Schrader, *Synth. Met.*, 1991, **41**, 831–836.
65 L. Groenendaal, F. Jonas, D. Freitag, H. Pielartzik and J. R. Reynolds, *Adv. Mater.*, 2000, **12**, 481–494.
66 H. Li, J. Cao, F. Liu, W. Zhou, X. Chen, Y. Deng, Z. Wu, B. Lu, D. Mo, J. Xu and G. Zhang, *ACS Appl. Energy Mater.*, 2022, **5**, 12315–12323.
67 S. Topal, I. Demirtas, E. Ertas, B. Ustamehmetoglu, E. Sezer and T. Ozturk, *ACS Appl. Energy Mater.*, 2023, **6**, 11532–11540.
68 E. G. C. Ergun, *ChemistrySelect*, 2025, 10(10), 202404423.
69 E. G. C. Ergun and A. M. Önal, *J. Energy Storage*, 2024, **104**, 114512.

70 E. G. Cansu Ergun and A. M. Önal, *Electrochim. Acta*, 2025, **510**, 145379.
71 Y. Tang, L. Zhang, S. Yan, Y. Kuai, H. Fu, W. Li, M. Ouyang and C. Zhang, *Solar Energy Materials and Solar Cells*, 2022, **245**, 111857.
72 H. Li, F. Liu, G. Zhang, W. Wang, W. Zhou, J. Xu, J. Zhang, B. Lu, Y. Zhang and L. Zhang, *J. Power Sources*, 2025, **633**, 236435.
73 K. Yin, Z. Yu, Y. Liu, S. Li, H. Guo, D. Zheng and J. Yu, *ACS Appl. Polym. Mater.*, 2025, **7**, 12459–12467.
74 D. Cevher, S. C. Cevher and A. Cirpan, *Dyes Pigments*, 2023, **218**, 111489.
75 S. Hosseini, Y. A. Udum and L. Toppare, *Electrochim. Acta*, 2025, **536**, 146667.
76 Y. Xie, Y. Zhang, M. Zhu, R. Huang and D. Chao, *Dyes Pigments*, 2022, **208**, 110889.
77 K. M. Kadish, K. M. Smith and Roger. Guilard, *The porphyrin handbook*, Academic Press, 2000, vol. 3.
78 P. J. Brothers and M. O. Senge, Eds., *Fundamentals of Porphyrin Chemistry*, Wiley, 2022.
79 N. U. Day, C. C. Wamser and M. G. Walter, *Polym. Int.*, 2015, **64**, 833–857.
80 H. Yin, T. Yang, K. Z. Wang, J. Tong and S. Y. Yu, *Langmuir*, 2019, **35**, 12620–12629.
81 K. A. Macor and T. G. Spiro, *J. Am. Chem. Soc.,* 1983, **105**, 5601–5607.
82 P. A. Liddell, M. Gervaldo, J. W. Bridgewater, A. E. Keirstead, S. Lin, T. A. Moore, A. L. Moore and D. Gust, *Chem. Mater.*, 2008, **20**, 135–142.
83 D. Schaming, I. Ahmed, J. Hao, V. Alain-Rizzo, R. Farha, M. Goldmann, H. Xu, A. Giraudeau, P. Audebert and L. Ruhlmann, *Electrochim. Acta*, 2011, **56**, 10454–10463.
84 A. Giraudeau, D. Schaming, J. Hao, R. Farha, M. Goldmann and L. Ruhlmann, *J. Electroanal. Chem.*, 2010, **638**, 70–75.
85 BettelheinV A, A. B. White, S. A. Raybuck and R. W. Murray, *Inorg. Chem.*, 1987, **26**, 1009–1017.
86 B. A. White and R. W. Murray, *J. Electroanal. Chem. Interfacial Electrochem.*, 1985, **189**, 345–352.
87 K. A. Macor, Y. O. Su, L. A. Miller and T. G. Spiro, *Inorg. Chem.*, 1987, **26**, 2594–2598.
88 K. A. Macor and T. G. Spiro, *J. Electroanal. Chem. Interfacial Electrochem.*, 1984, **163**, 223–236.
89 C. Paul-Roth, J. Rault-Berthelot, G. Simonneaux, J. Letessier and J. F. Bergamini, *J. Electroanal. Chem.*, 2007, **606**, 103–116.
90 A. Bettelheim, L. Soifer and E. Korin, *J. Electroanal. Chem.*, 2004, **571**, 265–272.
91 A. Bettelheim, D. Ozer, R. Harth and R. W. Murray, *J. Electroanal. Chem. Interfacial Electrochem.*, 1989, **266**, 93–108.
92 B. Ballarin, R. Seeber, L. Tassi and D. Tonelli, *Synth. Met.*, 2000, **114**, 279–285.
93 F. Zaar, S. Olsson, R. Emanuelsson, M. Strømme and M. Sjödin, *Electrochim. Acta*, 2022, **424**, 1406616–1406626.
94 J. Durantini, G. M. Morales, M. Santo, M. Funes, E. N. Durantini, F. Fungo, T. Dittrich, L. Otero and M. Gervaldo, *Org. Electron.*, 2012, **13**, 604–614.
95 M. G. Walter and C. C. Wamser, *J. Phys. Chem. C*, 2010, **114**, 7563–7574.
96 N. U. Day, M. G. Walter and C. C. Wamser, *J. Phys. Chem. C*, 2015, **119**, 17378–17388.
97 E. Tavakol, A. Kakekhani, S. Kavani, P. Tan, M. M. Ghaleni, M. A. Zaeem, A. M. Rappe and S. Nejati, *J. Am. Chem. Soc.*, 2019, **141**, 19560–19564.
98 S. Kochrekar, S. Sappati, P. K. Jha, E. Mäkilä, A. Jadhav, P. Damlin, M. Salomäki and C. Kvarnström, *J. Mater. Chem. C.*, 2025, **13**, 23577–23588.
99 S. M. Kuzmin, Svetlana A. Chulovskaya, Mariya V. Tesakova, Aleksandr S. Semeikin and Vladimir I. Parfenyuk, *J. Porphyrins Phthalocyanines*, 2017, **21**, 555–567.
100 S. M. Kuzmin, S. A. Chulovskaya, O. I. Koifman and V. I. Parfenyuk, *Electrochem. commun.*, 2017, **83**, 28–32.
101 S. M. Kuzmin, S. A. Chulovskaya and V. I. Parfenyuk, *J. Electroanal. Chem.* 2016, **772**, 80–88.

102 S. M. Kuzmin, S. A. Chulovskaya, O. A. Dmitrieva, N. Z. Mamardashvili, O. I. Koifman and V. I. Parfenyuk, *Journal of Electroanalytical Chemistry*, 2022, **918**, 116476.

103 Y. Guo, X. Hao, Y. Tao, C. Zhang and H. Cheng, *Synth. Met.*, 2019, **258**, 116202–116209.

104 M. Boudiaf, Y. Liang, R. Lamare, J. Weiss, H. Ibrahim, M. Goldmann, E. Bentouhami, V. Badets, S. Choua, N. Le Breton, A. Bonnefont and L. Ruhlmann, *Electrochim. Acta*, 2019, **309**, 432–449.

105 D. Schaming, A. Giraudeau, L. Ruhlmann, C. Allain, J. Hao, Y. Xia, R. Farha, M. Goldmann, Y. Leroux and P. Hapiot, *Oxidation of Porphyrins in the Presence of Nucleophiles: From the Synthesis of Multisubstituted Porphyrins to the Electropolymerization of the Macrocycles*. InTech, 2011, pp. 53–77.

106 Z. Huo, J. Gisselbrecht, R. Farha, M. Goldmann, E. Saint-aman, C. Bucher and L. Ruhlmann, *Electrochim. Acta,* 2014, **122**, 108–117.

107 Z. Huo, I. Azcarate, R. Farha, M. Goldmann, H. Xu, B. Hasenknopf, E. Lacôte and L. Ruhlmann, *J. Solid State Electrochem.*, 2015, **19**, 2611–2621.

108 D. Schaming, A. Giraudeau, S. Lobstein, R. Farha, M. Goldmann, J. P. Gisselbrecht and L. Ruhlmann, *J. Electroanal. Chem.*, 2009, **635**, 20–28.

109 A. Giraudeau, S. Lobstein, L. Ruhlmann, D. Melamed, K. M. Barkigia, and J. Fajer, *J. Porphyr. Phthalocyanines*, 2001, **5**, 793–797.

110 J. Hao, A. Giraudeau, Z. Ping, and L. Ruhlmann, *Langmuir*, 2008, **24**, 1600–1603.

111 S. Kochrekar, A. Kalekar, S. Mehta, P. Damlin, M. Salomäki, S. Granroth, N. Meltola, K. Joshi and C. Kvarnström, *RSC Adv.*, 2021, **11**, 19844–19855.

112 M. Lucero, M. Riquelme, G. Ramírez, M. C. Goya, A. G. Orive, A. H. Creus, M. C. Arévalo and M. J. Aguirre, *Int. J. Electrochem. Sci*, 2012, **7**, 234–250.

113 R. Arce, R. Del Río, D. Ruiz-León, J. Velez, M. Isaacs, M. A. Del Valle and M. J. Aguirre, *Int. J. Electrochem. Sci*, 2012, **7**, 11596–11608.

114 R. Arce, J. Romero and M. J. Aguirre, *J. Appl. Electrochem.*, 2014, **44**, 1361–1369.

115 S. Cogal, M. Kiristi, K. Ocakoglu, L. Oksuz and A. U. Oksuz, *Mater. Sci. Semicond. Process.*, 2015, **31**, 551–560.

116 M. Gervaldo, M. Funes, J. Durantini, L. Fernandez, F. Fungo and L. Otero, *Electrochim. Acta*, 2010, **55**, 1948–1957.

117 H. Zhang, Y. Zhang, C. Gu and Y. Ma, *Adv. Energy Mater.*, 2015, **5**, 1402175.

118 C. Zhang, Y. T. Xu, S. I. Sasaki and X. F. Wang, *Mater. Today Energy*, 2021, **21**, 100830.

119 C. Zhang, S. Duan, M. Zhou, Z. Liu, H. Ren, S. I. Sasaki and X. F. Wang, *Chem. Eng. J.*, 2022, **450**, 138000.

120 E. Bermúdez Prieto, E. J. González López, C. A. Solis, J. C. Leon Jaramillo, L. P. Macor, R. E. Domínguez, Y. B. Palacios, S. Bongiovanni Abel, E. N. Durantini, L. A. Otero, M. A. Gervaldo and D. A. Heredia, *RSC Adv.*, 2024, **14**, 15929–15941.

121 J. C. Leon Jaramillo, M. B. Boarini, S. Bongiovanni Abel, F. P. Cometto, T. M. Mondino, M. E. Milanesio, E. N. Durantini, L. A. Otero, M. A. Gervaldo and J. E. Durantini, *Batter. Supercaps*, 2026, **9**, 1–23.

122 J. E. Durantini, R. Rubio, C. Solis, L. Macor, G. M. Morales, M. I. Mangione, D. A. Heredia, E. N. Durantini, L. Otero and M. Gervaldo, *Sustain. Energy Fuels*, 2020, **4**, 6125–6140.

123 R. Rubio, M. B. Suarez, M. E. Pérez, D. A. Heredia, G. M. Morales, E. N. Durantini, L. Otero, M. Gervaldo and J. E. Durantini, *Electrochim. Acta*, 2023, **458**, 142552.

124 D. B. Papkovsky, G. V. Ponomarev and O. S. Wolfbeis, *Spectrochim. Acta A Mol. Biomol. Spectrosc.*, 1996, **52**, 1629–1638.

125 C. K. Chang and C. Sotiriou, *J. Heterocycl. Chem.*, 1985, **22**, 1739–1741.

126 P. E. Blöchl, *Phys. Rev. B*, 1994, **50**, 17953–17979.

127 D. Joubert, *Phys. Rev. B Condens. Matter Mater. Phys.*, 1999, **59**, 1758–1775.

128 S. Cosnier and A. Karyakin, *Electropolymerization: concepts, materials and applications*, Wiley-VCH, 2010.

129 M. G. Walter and C. C. Wamser, *J. Phys. Chem. C*, 2010, **114**, 7563–7574.
130 W. Zheng, N. Shan, L. Yu and X. Wang, *Dyes Pigments*, 2008, **77**, 153–157.
131 S. Trevin, F. Bedioui, M. G. G. Villegas and C. Bied-Charreton, *J. Mater. Chem.*, 1997, **7**, 923–928.
132 T. Kitagawa and Y. Ozaki, in *Metal Complexes with Tetrapyrrole Ligands I*, Springer-Verlag, Springer Berlin Heidelberg., 2005, pp. 71–114.
133 D. Wang, X. Cheng, Y. Shi, E. Sun, X. Tang, C. Zhuang and T. Shi, *Solid State Sci.*, 2009, **11**, 195–199.
134 L. M. C. Ferreira, D. Grasseschi, M. S. F. Santos, P. R. Martins, I. G. R. Gutz, A. M. C. Ferreira, K. Araki, H. E. Toma and L. Angnes, *Langmuir*, 2015, **31**, 4351–4360.
135 E. Mitraka, M. J. Jafari, M. Vagin, X. Liu, M. Fahlman, T. Ederth, M. Berggren, M. P. Jonsson and X. Crispin, *J. Mater. Chem. A Mater.*, 2017, **5**, 4404–4412.
136 R. Wu, M. Matta, B. D. Paulsen and J. Rivnay, *Chem. Rev.*, 2022, **122**, 4493–4551.
137 I. Zozoulenko, A. Singh, S. K. Singh, V. Gueskine, X. Crispin and M. Berggren, *ACS Appl. Polym. Mater.*, 2019, **1**, 83–94.
138 G. Louarn, M. Trznadel, J. P. Buisson, J. Laska, A. Pron, M. Lapkowski and S. Lefrant, *J. Phys. Chem.*, 1996, **100**, 12532–12539.
139 C. Castiglioni, M. Del Zoppo and G. Zerbi, *J. Raman Spectrosc.*, 1993, **24**, 485–494.
140 S. Garreau, G. Louarn, J. P. Buisson, G. Froyer and S. Lefrant, *Macromolecules*, 1999, **32**, 6807–6812.
141 J. Peng, Q. Lin, T. Földes, H.-H. Jeong, Y. Xiong, C. Pitsalidis, G. G. Malliaras, E. Rosta and J. J. Baumberg, *ACS Nano*, 2022, **16**, 21120–21128.
142 T. Yamaguchi, S. Hayashi and H. Ohtaki, *J. Phys. Chem.*, 1989, **93**, 2620–2625.
143 B. K. Thomas and D. J. Fray, *J. Appl. Electrochem.*, 1982, **12**, 1–5.

TURUN
YLIOPISTO
UNIVERSITY
OF TURKU

Painosalama, Turku, Finland 2026

ISBN 978-952-02-0735-9 (PRINT)
ISBN 978-952-02-0736-6 (PDF)
ISSN 0082-7002 (Print)
ISSN 2343-3175 (Online)